Table 2
Primer sequences of 51 genes examined in the study.

No.	Symbol	Left	Right	Ct
1	*Bax*	CCAGGATGCGTCCACCAAGAAG	GGAGTCCGTGTCCACGTCAGC	28
2	*Bcl2*	GATGACTTCTCTCGTCGCTACC	CATCCCTGAAGAGTTCCTCCAC	31
3	*Btg2*	ACGGGAAGAGAACCGACATGC	ATGATCGGTCAGTGCGTCCTG	24
4	*Casp1*	GTCTTGGAGACATCCTGTCAGG	GCATCTGTAGCCTAAATTCTGG	32
5	*Ccnf*	AGCACAAAGCCTTGCCACCATC	AAGCCAGGTGCGTGTCCTTGTC	25
6	*Ccng1*	TGGCCGAGATTTGACCTTCTGG	GTGCTTCAGTTGCCGTGCAGTG	22
7	*Ccng2*	GCCATCAAGCTAGGACTGTTAG	CACTTATCAACTCCATTCCCTG	26
8	*Cdkn1a (p21)*	TCCCGTGGACAGTGAGCAGTTG	CGTCTCCGTGACGAAGTCAAAG	22
9	*Cyp1a1*	TGGCCGATCGGAGGTCTTTC	AAGTGTTCACAGCGGGCGTG	29
10	*Cyp1a2*	GATGCTCTTCGGCTTGGGAAAG	CCATAGTTGGGTGTCAGGTCCAC	20
11	*Cyp4a10*	AGCCACAAGGGCAGTGTTCAGG	CCAAGCGGCCATTGGAAGAAAG	23
12	*Cyp21a1*	TGTGCTGCCCTTAAAGAAGAGTG	TTGAGCATCCCGTTCCCGTTTC	25
13	*Dpyd*	GTGCGGCTAAAGGCTGATGTGG	CCCATGGTTCACTGGTTTGCATG	24
14	*Egfr*	AGAACGCCTTCCACAGCCAC	ACTCTCGGAACTTTGGGCGG	22
15	*Ephx1*	CATTGTCTCCTCCCAGCGCTTC	GGGCATGCAGGATCTCAGAAGG	21
16	*Fabp5*	ACGGTCTGCACCTTCCAAGACG	ACCCGAGTGCAGGTGGCATTG	24
17	*Fos*	GTCGACCTAGGGAGGACCTTAC	CATCTCTGGAAGAGGTGAGGAC	31
18	*Gadd45b*	TGTACGAGGCGGCCAAACTG	TGTCGCAGCAGAACGACTGG	28
19	*Gadd45g*	GGAAAGCACAGCCAGGATGCAG	ATTCAGGACTTTGGCGGACTCG	26
20	*Gapdh*	GCTCTCAATGACAACTTTGTCAAG	CTTCCTTGGAGGCCATGTAGGC	22
21	*Gdf15*	AGCTGGAACTGCGCTTACGGG	CTCCAGCCCAAGTCTTCAAGAG	28
22	*Glul*	GGAATGGAGCAGGAATATACTC	ACCGCAGTAATACGGGCCTTG	22
23	*Gstk1*	CGTACTCCTGGCTGGGGCTTTG	CAGGTGGTTGGTTGCCGCTGTC	24
24	*Gyk*	GCCTGAAACAACTGCACTAGGC	CACAGCTTTCTTCCATGTGGAG	27
25	*Hist1h1c*	CGAGCTCATCACCAAGGCTGTG	CCCTTGCTCACCAGGCTCTTC	26
26	*Hspa1b (Hsp70)*	GACAAGTCGGAGAACGTGCAG	CGAGTAGGTGGTGAAGGTCTG	25
27	*Hspb1*	CGGTGCTTCACCCGGAAATAC	GCTGACTGCGTGACTGCTTTGG	25
28	*Hspb2 (Hsp27)*	CTCACAGTGAAGACCAAGGAAG	GGATAGGGAAGAGGACACTAGG	26
29	*Hmox1*	AAGACCGCCTTCCTGCTCAAC	CGAAGTGACGCCATCTGTGAGG	28
30	*Hprt1*	CTTGCTCGAGATGTCATGAAGGAG	TAATCCAGCAGGTCAGCAAAGAAC	26
31	*Igfbp1*	GATCAGCCCATCCTGTGGAACG	TTCTCGTTGGCACGGCTCCTTC	24
32	*Isg20l1*	TTGAAGGGCAAGGTGGTGGTG	GAGCAGGTTTGGGACATAAGTG	24
33	*Jun*	GCCAAGAACTCGGACCTTCTC	AGTGGTGATGTGCCCATTGCTG	23
34	*Kras*	GGCAAGAGCGCCTTGACGATAC	TGGTCCCTCATTGCACTGTACTCC	28
35	*Lig3*	TGCGGCTCTACTTGCCACCTTC	CATGTGTGGCTGAGCCCATGTC	27
36	*Lrp1*	GGGCCATGAATGTGGAAATTGG	GTGGCATACACTGGGTTGGTG	22
37	*Mbd1*	GGATCCTGACACTCAAGAATGG	GTTTGGGCTAACACAGGAAGAG	23
38	*Mdm2*	TTGATCCGAGCCTGGGTCTGTG	AAGATCCTGATGCGAGGGCGTC	27
39	*Myc*	B5.6TCAGCAACAACCGCAAGTGCTC	AAAGCTGCGCTTCAGCTCGTTC	32
40	*Net1*	GACCTCCACGAAGAGTGTGAAG	CTGTACACTGGAGCCACAATCC	27
41	*Pdgfb*	AAGACGCGCACAGAGGTGTTCC	GGCATTGCACATTGCGGTTATTG	33
42	*Plk2*	CTGTTGAGAGCGTCTTCAGTTG	CCATAGTTCACAGTTAAGCAGC	28
43	*Pml*	GGCAAGAAGCGTCCTTACCTTC	GGACAGCAACAGCAGTTCAGTC	28
44	*Pmm1*	TGTCCCGAGGAGGCATGATAAG	CAAAGTCATTCCCGCCAGGAC	30
45	*Ppp1r3c*	TGGAAACCTGACGGAGTGCAG	GCAAGCCTTGGACTGCCAAAG	24
46	*Rad52*	TGACGCCACTCACCAGAGGAAG	GCTGGAAGTACCGCATGCTTGG	30
47	*Rcan1*	GGTCCACGTGTGTGAGAGTG	TGGATGGGTGTGTACTCCGG	24
48	*Trp53*	TTGGACCCTGGCACCTACAATG	GCAGACAGGCTTTGCAGAATGG	26
49	*Tubb2c*	TTGGCAACAGCACCGCTATTC	TCGGACACCAGGTCGTTCATG	23
50	*Ube2e1 (UbcM3)*	AACTGGAGCCCAGCCCTAACC	TGGCCATTCTGTCGTGTTCTGC	24
51	*Ung*	AACCTGAGTGGCCTCGTCTTCC	TCTGCATCCCAGGAACCCTCTG	29

Ct values are those of the highest group in the present experimental condition.

At 28 days, three DEN-28 d-Grp-1 genes showed a dose-dependent increase of more than four-fold. Seventeen DEN-28 d-Grp-2 genes were suggested to have a gradual dose-dependent increase, though less than that for the expression in DEN-28 d-Grp-1. Ungrouped *Igfbp1* showed a dose-dependent decrease of less than 0.3-fold.

Unsupervised *k*-means clustering results are shown in Fig. 3A. Genes were classified into four clusters based on the hierarchical clustering results. Gene expression was classified into four clusters (DEN-4 h-Cluster-1 to DEN-4 h-Cluster-4) 4 h after administration, and four clusters (DEN-28 d-Cluster-1 to DEN-28 d-Cluster-4) 28 days after administration. As unsupervised *k*-means clustering was performed for 4 h and 28-day data separately, cluster member genes were different for 4 h and 28 days.

At 4 h, all 12 DEN-4 h-Cluster-1 genes exhibited a dose-dependent increase of more than eight-fold. Fourteen DEN-4 h-Cluster-2 genes showed a gradual dose-dependent increase as compared to DEN-4 h-Cluster-1 genes. Although *Myc* and *Igfbp1* in DEN-4 h-Cluster-3 had some atypical dose–response, they showed an increase of up to or greater than two-fold, as a whole. Two genes in DEN-4 h-Cluster-4 exhibited a dose-dependent decrease of less than 0.3-fold [*Cyp1a2* and *Glul*]. For 28-day data, 4 DEN-28 d-Cluster-1 genes showed a dose-dependent increase of more than two-fold. *Igfbp1* in DEN-28 d-Cluster-3 showed a dose-dependent decrease of less than 0.3-fold.

Two types of clustering results for the DEN data are summarized as follows. A total of 28 genes showed a dose-dependent increase or decrease at 4 h or 28 days after administration. Twenty-six genes in DEN-4 h-Grp-1 or DEN-4 h-Grp-2 and DEN-4 h-Cluster-1, DEN-4 h-Cluster-2 or DEN-4 h-Cluster-3 showed a dose-dependent increase ranging from 2-fold to more than 64-fold [*Bax*, *Btg2*, *Ccng1*, *Ccng2*, *Cdkn1a*, *Cyp4a10*, *Cyp21a1*, *Fos*, *Gadd45b*, *Gdf15*, *Hspb1*, *Hmox1*, *Hsp27*, *Igfbp1*, *Isg20l1*, *Jun*, *Mbd1*, *Mdm2*, *Myc*, *Net1*, *Plk2*, *Pmm1*, *Ppp1r3c*, *Rad52*, *Rcan1* and *Tubb2c*]. Two genes in DEN-4 h-Grp-4

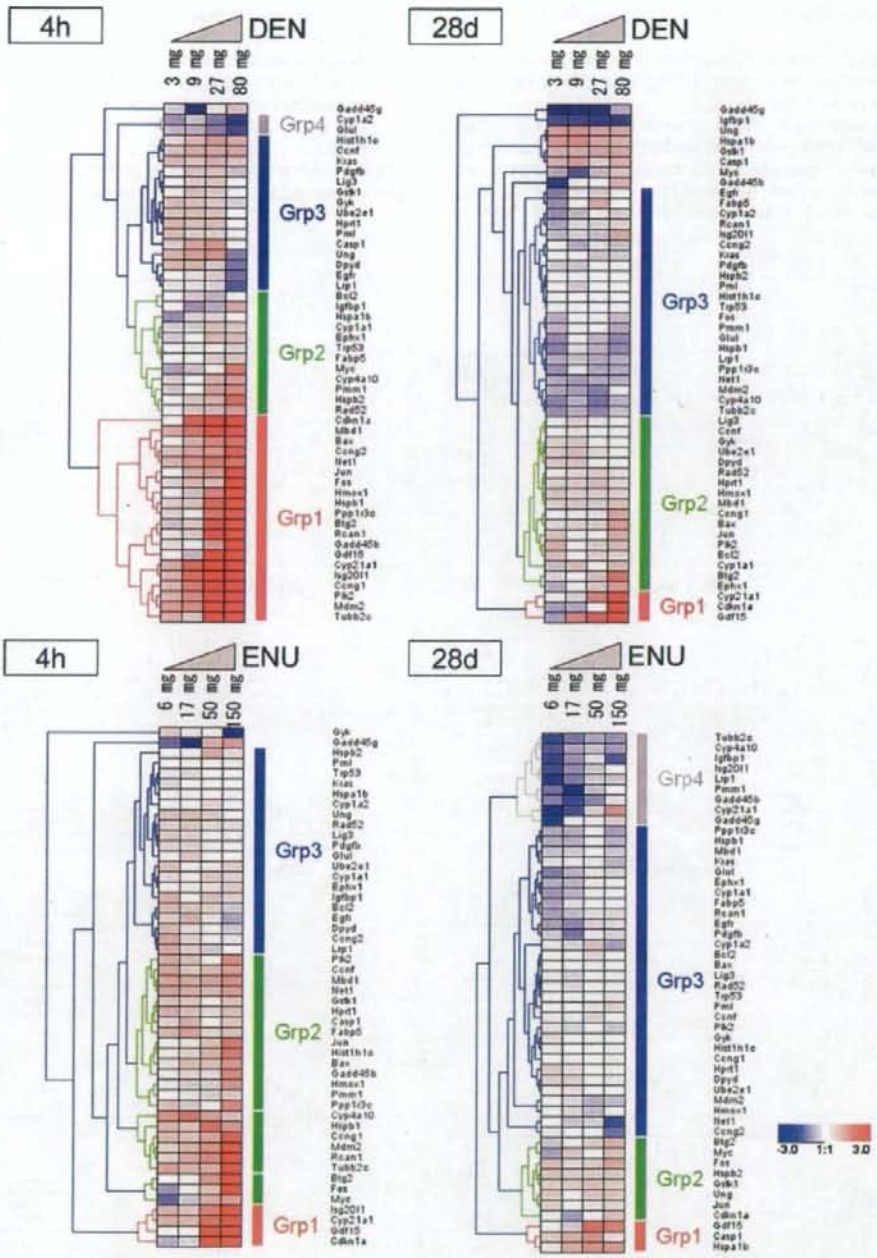

Fig. 2. Cluster analysis of gene expression after DEN and ENU treatment. The expression of 50 genes was clustered by hierarchical clustering after DEN or ENU treatment. Results of 4 h and 28 days were analyzed separately. The color displays show the $\log_2$ (expression ratio) as (1) red when the treatment sample is up-regulated relative to the control sample, (2) blue when the treatment sample is down-regulated relative to the control sample and (3) white when the $\log_2$ (expression ratio) is close to zero.

and DEN-4 h-Cluster-4 showed a dose-dependent decrease of less than 0.3-fold [*Cyp1a2* and *Glul*].

At 28 days, four genes in DEN-28 d-Grp-1 or DEN-28 d-Grp-2 and DEN-28 d-Cluster-1, which showed a dose-dependent increase at 4 h, also showed a dose-dependent increase by more than 2–4-fold [*Btg2*, *Cdkn1a*, *Cyp21a1* and *Gdf15*]. *Igfbp1* in the ungrouped group and DEN-28 d-Cluster-3 showed a dose-dependent decrease of less than 0.3-fold.

3.1.2. Identification of biologically relevant networks for DEN treatment

DEN numerical data of all 51 examined genes were analyzed by IPA, and 5 gene networks were extracted (Table 3). Five networks are also shown as bar graphs in Fig. 4.

For the 4 h time point, 35 genes were extracted in DEN-4 h-Network-1 (cancer, cell cycle and reproductive system disease); of these, 15 genes were examined in this study, and 11 of these genes showed a dose-dependent response [*Bax*, *Btg2*, *Ccng1*, *Cdkn1a*, *Gadd45b*, *Gdf15*, *Hspb1*, *Hspb2*, *Mdm2*, *Plk2* and *Pmm1*] (Fig. 4A, Network-1). Network-1 was a highly active network for DEN-4 h. *Trp53* and *Cdkn1a* appeared to be core genes in DEN-4 h-Network-1. *Trp53* has 15 associations [*Bax*, *Btg2*, *Casp1*, *Ccng1*, *Cdkn1a*, *Gadd45 complex*, *Gdf15*, *Hist1h1c*, *Hspb1*, *Mdm2*, *Plk2*, *Pml*, *Pmm1*, *Pdgf* complex and *Caspase* complex], and *Cdkn1a* has 9 associations [*Trp53*, *Plk2*, *Pdgf complex*, *Gdf15*, *Gadd45b*, *Gadd45g*, *Mdm2*, *Caspase* complex and *Pml*].

DEN-4 h-Network-2 (cell cycle, DNA replication, recombination, repair and cell death) consisted of 35 genes, 15 of which were examined in this study; 11 of these genes showed a dose-dependent

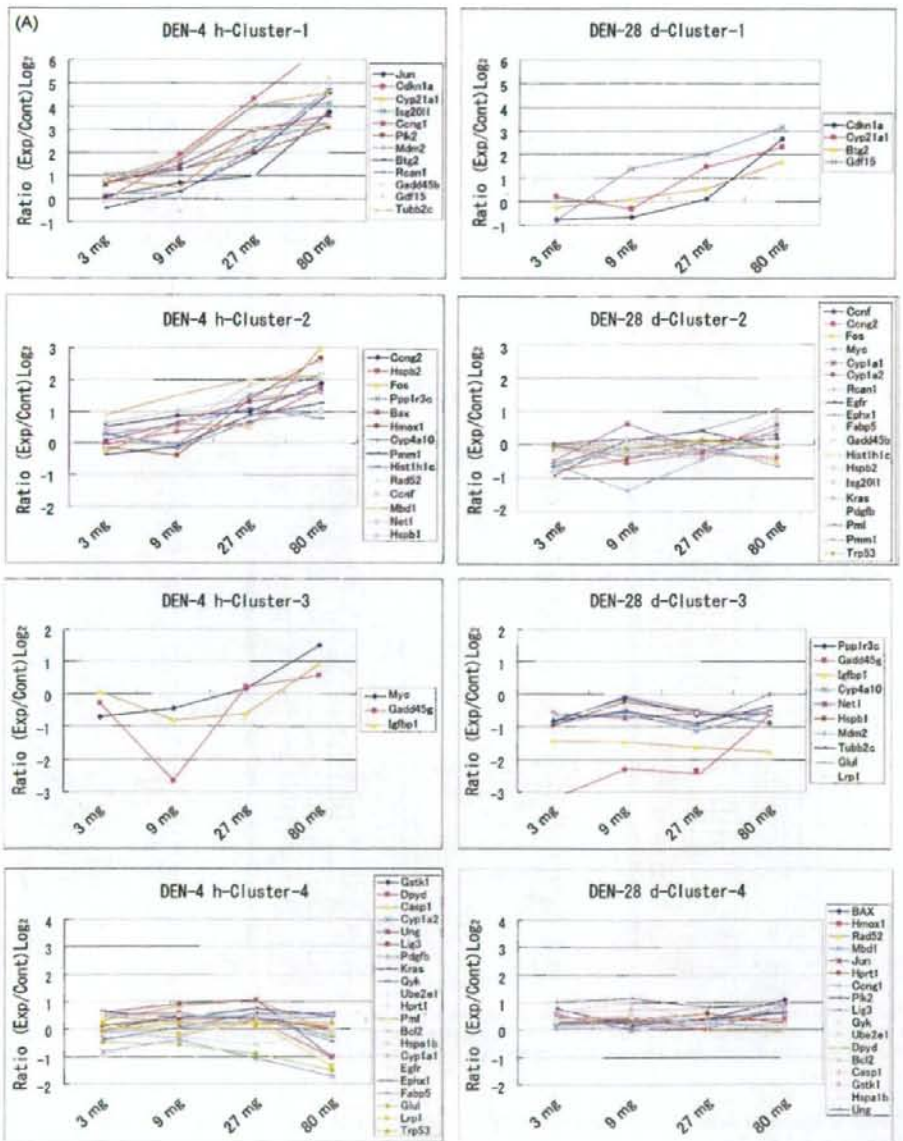

Fig. 3. Cluster analysis and dose-dependent expression pattern. The expression of 50 genes was clustered by *k*-means clustering after (A) DEN or (B) ENU treatment. Results of 4 h and 28 days were analyzed separately.

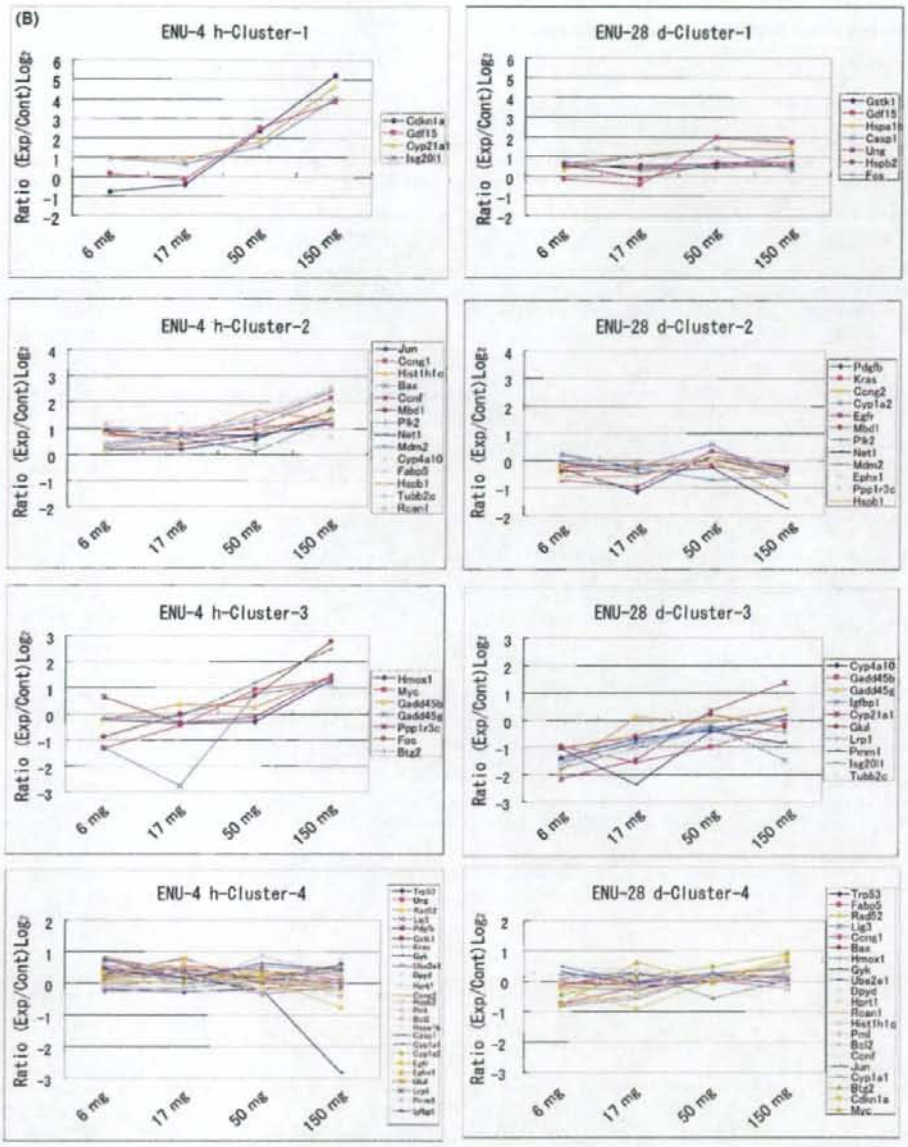

Fig. 3. (*Continued*).

response [*Ccng2*, *Cyp1a2*, *Cyp4a10*, *Cyp21a1*, *Gdf15*, *Glul*, *Igfbp1*, *Ppp1r3c Rad52*, *Rcan1* and *Tubb2c*] (Fig. 4A, Network-2). Network-2 was also a highly active network for DEN-4 h. *Il1b* and *Sp1* seemed to be core genes in DEN-4 h-Network-2. *Il1b* has five associations [*Gdf15*, *Fabp5*, *Rcan1*, *Igfbp1* and *Hprt1*], and *Sp1* has three associations [*Gdf15*, *Igfbp1* and *Cyp21a1*].

DEN-4 h-Network-3 (liver necrosis/cell death and hepatic system disease) consisted of 36 genes, 10 of which were examined in this study; 5 of these genes showed a dose-dependent response [*Fos*, *Hmox1*, *Jun*, *Myc* and *Net1*) (Fig. 4A, Network-3).

DEN-4 h-Network-4 (cell cycle, DNA replication, recombination, repair and cell death) consisted of 35 genes, 9 of which were examined in this study; 2 of these genes [*Isg20l1* and *Mbd1*] showed a dose-dependent response (Fig. 4A, Network-4).

DEN-4 h-Network-5 (cancer, drug metabolism and genetic disorder) consisted of two genes, neither of which showed a dose-dependent response in this study (Fig. 4A, Network-5).

For 28-day data, DEN-28 d-Network-1 consisted of the same genes and the same top functions as for DEN-4 h-Network-1 (Table 3(B)); however, a generally lower dose-dependent response

Table 3
Gene networks and their primary functions after DEN and ENU treatment.

Networks	Molecules in network	Top functions
(A) DEN 4 h		
1	Adaptor protein 2, Ahr-aryl hydrocarbon-*Arnt*, *Arf*, ***Bax***, ***Btg2***, *Casp1*, Caspase, *Cbp/p300*, ***Ccng1***, ***Cdkn1a***, *Creb*, Cyclin A, Cyclin E, *E2f*, *Erk1/2*, *Gadd45*, ***Gadd45b***, *Gadd45g*, ***Gdf15***, *Gsk3*, *Hist1h1c*, ***Hspb1***, ***Hspb2***, *Jun/Junb/Jund*, ***Mdm2***, *Mek1/2*, *Pak*, *Pdgf*, ***Plk2***, *Pml*, ***Pmm1***, *Pp2a*, *Rb*, *Stat*, *Trp53*	Cancer, Cell cycle, reproductive system disease
2	*Aatf*, *Aldh3a1*, *App*, beta-estradiol, *Ccne2*, ***Ccng2***, ***Cyp1a2***, ***Cpy21a1***, ***Cyp4a10***, *E2F1*, *Fabp5*, ***Gdf15***, *Gyk*, ***Glul***, *Hprt1*, *Hspa1b*, ***Igfbp1***, *Igfbp7*, *Il10*, *Il1b*, *Irf2*, *Klf10*, *MAZ*, *Meis1*, *Muc2*, ***Ppp1r3c***, ***Rad52***, ***Rcan1***, retinoic acid, *Scye1*, *Sp1*, *St8sia1*, *Tgm1*, *TopbpPT*, ***Tubb2c***	Cell cycle, DNA replication, recombination, and repair, cell death
3	*Akt*, *Ap1*, *Bcl2*, Calpain, *Egfr*, *Fgf*, ***Fos***, *Fos-Jun*, ***Hmox1***, *Ige*, *Il1*, *Jnk*, ***Jun***, *Kras*, *Lig3*, *Mapk*, *Mek*, *Mmp*, ***Myc***, ***Net1***, *P38*, *Mapk*, *Pdgf bb*, *Pdgfb*, *Pi3k*, *Pkc(s)*, *Pkg*, *Rar*, *Ras*, *Ras* homolog, *Rock*, *Rxr*, *Sos*, *Stat5a/b*, *Tgf* beta, *Vegf*	Cell death, hepatic system disease, liver necrosis/cell death
4	4-Phenylbutyric acid, *14-3-3*, Calmodulin, *Ccnf*, *Cdkn2a*, *Ck2*, *Cult1*, Cyclin D, *Cyp1a1*, *Ephx1*, *Hira*, Histone h3, *Hnrpa2b1*, *Hsp70*, *Hsp90*, *Hspa1b*, hydrogen peroxide, *Ifng*, *Irf2*, ***Isg20l1***, lipoxin A4, *Lrp1*, ***Mbd1***, *Mcm2*, *Mcm3*, *Meis1*, *Pdk1*, *Pka*, RNA polymerase II, *Ssrp1*, *Supt16h*, *Tp53inp1*, *Ube2e1*, Ubiquitin, *Ung*	Cell cycle, DNA replication, recombination, and repair, cell death
5	*Cdh3*, D *Dpyd*	Cancer, drug metabolism, genetic disorder
(B) DEN 28 d		
1	Adaptor protein 2, Ahr-aryl hydrocarbon-*Arnt*, *Arf*, *Bax*, ***Btg2***, *Casp1*, Caspase, *Cbp/p300*, *Ccng1*, ***Cdkn1a***, *Creb*, Cyclin A, Cyclin E, *E2f*, *Erk1/2*, *Gadd45*, *Gadd45b*, *Gadd45g*, ***Gdf15***, *Gsk3*, *Hist1h1c*, *Hspb1*, *Hspb2*, *Jun/Junb/Jund*, *Mdm2*, *Mek1/2*, *Pak*, *Pdgf*, *Plk2*, *Pml*, *Pmm1*, *Pp2a*, *Rb*, *Stat*, *Trp53*	Cancer, cell cycle, reproductive system disease
2	*Aatf*, *Aldh3a1*, *App*, beta-estradiol, *Ccng2*, *Cyp1a2*, ***Cyp21a1***, *Cyp4a10* (includes EG:1579), *E2f1*, *Fabp5*, ***Gdf15***, *Gyk*, *Glul*, *Hrpt1*, *Hspa1b*, ***Igfbp1***, *Il10*, *Il1b*, *Klf10*, *Klk5*, *Maz*, *Meis1*, *Mt1e*, *Muc2*, *Nr4a3*, *Ppp1r3c*, *Rad52*, *Rcan1*, retinoic acid, *Scye1*, *Sp1*, *St8sia1*, *Tgm1*, *Topbp1*, *Tubb2c*	DNA replication, recombination, and repair, cell death, cell cycle
3	*Akt*, *Ap1*, *Bcl2*, Calpain, *Egfr*, *Fgf*, *Fos*, *Fos-Jun*, *Hmox1*, *Ige*, *Il1*, *Jnk*, *Jun*, *Kras*, *Lig3*, *Mapk*, *Mek*, *Mmp*, *Myc*, *Net1*, *P38 Mapk*, *Pdgf bb*, *Pdgfb*, *Pi3k*, *Pkc(s)*, *Pkg*, *Rar*, *Ras*, *Ras* homolog, *Rock*, *Rxr*, *Sos*, *Stat5a/b*, *Tgf* beta, *Vegf*	Cell death, hepatic system disease, liver necrosis/cell death
4	*14-3-3*, *Bag4*, Calmodulin, *Ccnf*, *Cdkn2a*, *Ck2*, *Cutl1*, *Cyp1a1*, *Dynlrb1*, *Ephx1*, *Hira*, Histone h3, *Hnrpa2b1*, *Hoxb9*, *Hsp70*, *Hsp90*, *Hspa1b*, hydrogen peroxide, *Ifng*, *Isg20l1*, *Lrp1*, *Mbd1*, *Meis1*, *Nol3*, *Pdk1*, *Pka*, *Ppfibp1*, RNA pol2-transcription factor, RNA polymerase II, *Smtn*, *Supt16h*, *Tp53inp1*, *Ube2e1*, Ubiquitin, *Ung*	Cellular development, cellular growth and proliferation, connective tissue development and function
5	*Cdh3*, *Dpyd*	Cancer, drug metabolism, genetic disorder
(C) ENU 4 h		
1	Adaptor protein 2, Ahr-aryl hydrocarbon-*Arnt*, *Arf*, ***Bax***, ***Btg2***, *Casp1*, Caspase, *Cbp/p300*, ***Ccng1***, ***Cdkn1a***, *Creb*, Cyclin A, Cyclin E, *E2f*, *Erk1/2*, *Gadd45*, ***Gadd45b***, *Gadd45g*, ***Gdf15***, *Gsk3*, ***Hist1h1c***, ***Hspb1***, *Hspb2*, *Jun/Junb/Jund*, ***Mdm2***, *Mek1/2*, *Pak*, *Pdgf*, ***Plk2***, *Pml*, *Pmm1*, *Pp2a*, *Rb*, *Stat*, *Trp53*	Cancer, cell cycle, reproductive system disease
2	*Aatf*, *Aldh3a1*, *App*, *Appbp1*, beta-estradiol, *Ccne2*, *Ccng2*, *Cyp1a2*, ***Cyp21a1***, ***Cyp4a10***, *E2f1*, ***Fabp5***, ***Gdf15***, *Gyk*, *Glul*, *Hprt1*, *Hdps1b*, *Igfbp1*, *Il10*, *Il1b*, *Klf10*, *Maz*, *Mis1*, *Muc2*, *Nr4a3*, ***Ppp1r3c***, *Rad52*, ***Rcan1***, retinoic acid, *Scye1*, *Sp1*, *St8sia1*, *Tgm1*, *Topbp1*, ***Tubb2c***	DNA replication, recombination, and repair, cell cycle, cell signaling
3	*Akt*, *Ap1*, *Bcl2*, Calpain, *Egfr*, *Fgf*, ***Fos***, *Fos-Jun*, ***Hmox1***, *Ige*, *IL1*, *Jnk*, ***Jun***, *Kras*, *Lig3*, *Mapk*, *Mek*, *Mmp*, ***Myc***, ***Net1***, *P38*, *Mapk*, *Pdgf bb*, *Pdgfb*, *Pi3k*, *Pkc(s)*, *Pkg*, *Rar*, *Ras*, *Ras* homolog, *Rock*, *Rxr*, *Sos*, *Stat5a/b*, *Tgf* beta, *Vegf*	Cell death, hepatic system disease, liver necrosis/cell death
4	4-phenylbutyric acid, *14-3-3*, Calmodulin, ***Ccnf***, *Cdkn2a*, *Ck2*, *Cult1*, Cyclin D, *Cyp1a1*, *Ephx1*, *Hira*, Histone h3, *Hnrpa2b1*, *Hsp70*, *Hsp90*, *Hspa1b*, hydrogen peroxide, *Ifng*, *Irf2*, ***Isg20l1***, lipoxin A4, *Lrp1*, ***Mbd1***, *Mcm2*, *Mcm3*, *Meis1*, *Pdk1*, *Pka*, RNA polymerase II, *Ssrp1*, *Supt16h*, *Tp53inp1*, *Ube2e1*, Ubiquitin, *Ung*	Cell cycle, DNA replication, recombination, and repair, cell death
5	*Cdh3*, *Dpyd*	Cancer, drug metabolism, genetic disorder
(D) ENU 28 d		
1	Adaptor protein 2, Ahr-aryl hydrocarbon-*Arnt*, *Arf*, *Bax*, *Btg2*, ***Casp1***, Caspase, *Cbp/p300*, *Ccng1*, *Cdkn1a*, *Creb*, Cyclin A, Cyclin E, *E2f*, *Erk1/2*, *Gadd45*, *Gadd45b*, *Gadd45g*, ***Gdf15***, *Gsk3*, *Hist1h1c*, *Hspb1*, ***Hspb2***, *Jun/Junb/Jund*, *Mdm2*, *Mek1/2*, *Pak*, *Pdgf*, *Plk2*, *Pml*, *Pmm1*, *Pp2a*, *Rb*, *Stat*, *Trp53*	Cancer, cell cycle, reproductive system disease
2	*Aatf*, Ahr-aryl hydrocarbon, *App*, *Appbp1*, beta-estradiol, *Ccng2*, *Cd68*, *Cdc45l*, *Cyp1a2*, *Cyp21a1*, *Cyp4a10*, *E2f1*, *Fabp5*, *Folr2*, ***Gdf15***, *Gyk*, *Glul*, *Hprt1*, ***Hspa1b***, *Igfbp1*, *Il10*, *Il1b*, *Klk5*, *Krt16*, *Nr4a3*, *Ppp1r3c*, *Rad52*, *Rcan1*, retinoic acid, *Krs4x*, *Serpinb9*, *Sp1*, *TacstdA1*, *Tspo*, *Tubb2c*	Cell signaling, molecular transport, small molecule biochemistry
3	*Akt*, *Ap1*, *Bcl2*, Calpain, *Egfr*, *Fgf*, ***Fos***, *Fos-Jun*, *Hmox1*, *Ige*, *IL1*, *Jnk*, *Jun*, *Kras*, *Lig3*, *Mapk*, *Mek*, *Mmp*, *Myc*, ***Net1***, *P38*, *Mapk*, *Pdgf bb*, *Pdgfb*, *Pi3k*, *Pkc(s)*, *Pkg*, *Rar*, *Ras*, *Ras* homolog, *Rock*, *Rxr*, *Sos*, *Stat5a/b*, *Tgf* beta, *Vegf*	Cell death, hepatic system disease, liver necrosis/cell death
4	*14-3-3*, *Aco1*, *Asf1b*, *Bag4*, Calmodulin, *Ccnf*, *Cdkn2a*, *Ck2*, *Cyp1a1*, *Dynlrb1*, *Ephx1*, *Hira*, Histone h3, *Hosb9*, *Hsp70*, *Hsp90*, ***Hspa1b***, hydrogen peroxide, *Ifng*, *Isg20l1*, *Lamp1*, *Lrp1*, *Mbd1*, *Nol3*, *Pka*, *Ppfibp1*, RNA pol2-transcription factor, RNA polymerase II, *Rpl21*, *Smtn*, *Sncg*, *Supt16h*, *Ube2e1*, Ubiquitin, ***Ung***	Cellular development, cellular growth and proliferation, connective tissue development and function
5	*Cdh3*, *Dpyd*	Cancer, drug metabolism, genetic disorder

Biologically relevant networks extracted by IPA are shown for gene expression data after (A) DEN-4 h, (B) DEN-28 d, (C) ENU-4 h or (D) ENU-28 d treatment. Bold underlined genes show dose-dependent expression. Thin underlined genes are genes examined in the present study. *Pdgf bb* in Network-3 means *Pdgf* groups of *Pdgfa*, *Pdgfb*, *Pdgfc* and *Pdgfd*. *Hsp70* in Network-4 means *Hsp* groups of *Hspa14 hspa1a*, *Hspa1b*, *Hspa1l*, *Hspa2*, *Hspa4 hspa5*, *Hspa6*, *Hspa7*, *Hspa8*, and *Hspa9*.

was observed, and only *Btg2*, *Cdkn1a* and *Gdf15* showed a dose-dependent increase (Fig. 4A, Network-1). DEN-28 d-Network-2 included several different genes from those in DEN-4 h-Network-2 but had the same primary functions as for DEN-4 h-Network-2, and *Cyp21a1*, *Gdf15* and *Igfbp1* exhibited dose-dependency (Fig. 4A, Network-2). DEN-28 d-Network-3 consisted of the same genes and the same primary functions as for DEN-4 h-Network-3; however, no genes showed dose-dependency (Fig. 4A, Network-3). DEN-28 d-Network-4 contained a few different genes and primary functions from those of DEN-4 h-Network-4, but no genes showed a dose

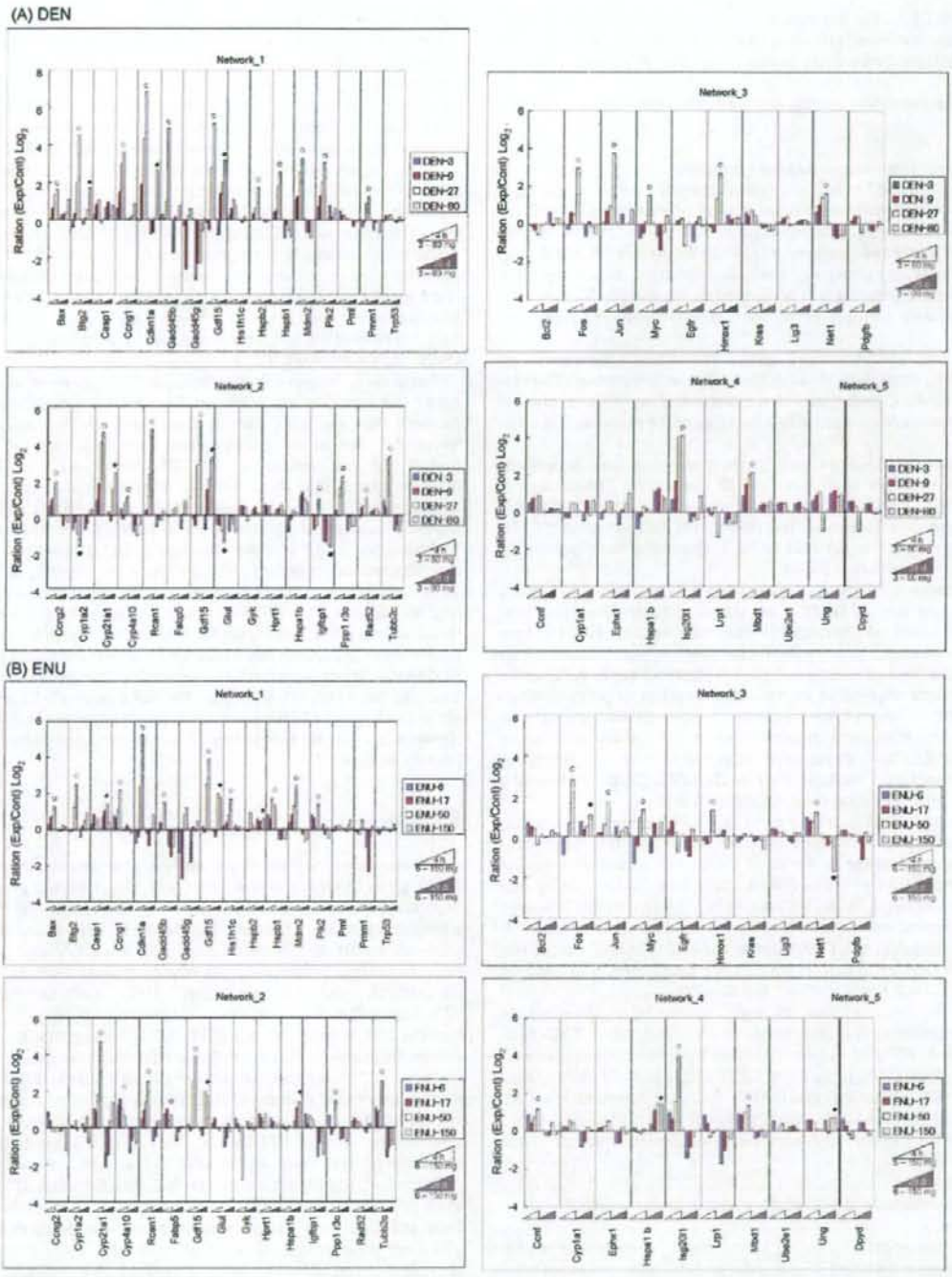

Fig. 4. Dose-dependent gene expression in each network based on different time points. The ratio values (log_2) of genes in each network are shown as bar graphs for DEN treatment (A) or ENU treatment (B). ○ shows a dose-dependent increase at 4 h, ♦ shows a dose-dependent increase at 28 days and ● shows a dose-dependent decrease.

response. DEN-28 d-Network-5 consisted of the same genes and the same top functions as those of DEN-4 h-Network-5, with no genes showing dose-dependency in this study (Fig. 4A, Network-5).

3.2. Dose-dependent alteration of gene expression induced with ENU

3.2.1. Clustering analysis for gene expression

Unsupervised hierarchical clustering results are shown in Fig. 2. The clustering presented three groups (ENU-4 h-Grp-1 to ENU-4 h-Grp-3) and two ungrouped genes for the 4 h time point after administration and four groups (ENU-28 d-Grp-1 to ENU-28 d-Grp-4) for the 28-day time point after administration. As unsupervised hierarchical clustering was performed on 4 h and 28-day data separately, group member genes were different between these two groups.

All four ENU-4 h-Grp-1 genes showed a dose-dependent increase by more than 16–32-fold 4 h after administration. Twenty-four ENU-4 h-Grp-2 genes were suggested to have a gradual dose-dependent increase of less than that of the expression in ENU-4 h-Grp-1.

All three ENU-28 d-Grp-1 genes showed a dose-dependent increase by more than two-fold 28 days after administration. Eight ENU-28 d-Grp-2 genes were suggested to have a gradual dose-dependent increase of less than that of the expression in ENU-28 d-Grp-1. *Net1* in ENU-28 d-Grp-3 showed a dose-dependent decrease of less than 0.3-fold.

Unsupervised *k*-means clustering results are shown in Fig. 3B. In the same way as for DEN, we classified these genes into four clusters based on hierarchical clustering results. For 4 h, four ENU-4 h-Cluster-1 genes exhibited a dose-dependent increase by more than 16-fold. Fourteen ENU-4 h-Cluster-2 genes exhibited a gradual dose-dependent increase as compared to genes in ENU-4 h-Cluster-1. Seven ENU-4 h-Cluster-3 genes showed an increase as a whole, with some atypical features. For 28-day data, seven ENU-28 d-Cluster-1 genes were suggested to have a tendency for a dose-dependent increase. *Net1* in ENU-28 d-Cluster-2 showed a dose-dependent decrease of less than 0.3-fold.

Two kinds of clustering results of ENU treatment are summarized as follows. A total of 29 genes showed a dose-dependent increase or decrease at 4 h or 28 days after administration. For 4 h, a total of 24 genes in ENU-4 h-Grp-1 or ENU-4 h-Grp-2 and ENU-4 h-Cluster-1, ENU-4 h-Cluster-2 or ENU-4 h-Cluster-3 showed a dose-dependent increase ranging from 2-fold to more than 32-fold [*Bax, Btg2, Ccng1, Ccnf, Cdkn1a, Cyp4a10, Cyp21a1, Fabp5, Fos, Gadd45b, Gdf15, Hist1h1c, Hmox1, Hspb1, Isg20l1, Jun, Mbd1, Mdm2, Myc, Net1, Plk2, Ppp1r3c, Rcan1* and *Tubb2c*].

For 28 days, a total of eight genes were classified as dose–response genes. Four genes in ENU-28 d-Grp-1, ENU-28 d-Grp-2, and ENU-28 d-Cluster-1 showed a dose-dependent increase of more than 2-fold [*Casp1, Fos, Gdf15* and *Hspa1b*]. Another three genes in ENU-28 d-Grp2 and ENU-28 d-Cluster-1 showed less than a two-fold increase [*Gstk1, Hspb2* and *Ung*]. *Net1* in ENU-28 d-Grp-3 and ENU-28 d-Cluster-2 showed a dose-dependent decrease of less than 0.3-fold.

3.2.2. Identification of biologically relevant networks for ENU treatment

ENU numerical data for all 51 examined genes were also analyzed by IPA for 4 h and 28-day data, and five gene networks were extracted (3). In total, the gene expression pattern for ENU was similar to the pattern for DEN; however, some differences were observed.

For 4 h, ENU-4 h-Network-1 consisted of the same genes and the same top functions as for DEN-4 h-Network-1, and 10 of these genes showed a dose-dependent increase [*Bax, Btg2, Ccng1, Cdkn1a, Gadd45b, Gdf15, Hist1h1c, Hspb1, Mdm2* and *Plk2*] (Fig. 4B, Network-1). Network-1 was the most active network for ENU-4 h. ENU-4 h-Network-2 (DNA replication, recombination, repair, cell cycle and cell signaling) included a different primary function from that of DEN-4 h-Network-2 and a few different genes from those for DEN, and seven genes showed a dose-dependent increase [*Cyp21a1, Cyp4a10, Fabp5, Gdf15, Ppp1r3c, Rcan1* and *Tubb2c*] (Fig. 4B, Network-2). ENU-4 h-Network-3 consisted of the same genes and the same top functions as those for DEN-4 h-Network-3, and five genes showed a dose-dependent increase [*Fos, Hmox1, Jun, Myc* and *Net1*] (Fig. 4B, Network-3). ENU-4 h-Network-4 also consisted of the same genes and the same top functions as those for DEN, and three genes showed a dose-dependent increase [*Ccnf, Isg20l1* and *Mbd1*] (Fig. 4B, Network-4). ENU-4 h-Network-5 consisted of the same genes and the same top functions as those for DEN-4 h-Network-5, but no genes showed a dose–response in this study (Fig. 4B, Network-5).

Network-1, Network-3 and Network-5 consisted of common genes and common top functions for both 4 h and 28 days and for both DEN and ENU. For 28 days, three genes in ENU-28 d-Network-1 showed a dose-dependent increase [*Casp1, Gdf15* and *Hspb2*] (Fig. 4B, Network-1). ENU-28 d-Network-2 included 10 different genes from those for ENU-4 h-Network-2 and had different top functions (cell signaling, molecular transport and small molecule biochemistry) from those of DEN-4 h-Network-2, DEN-28 d-Network-2 and ENU-4 h-Network-2, and 2 genes showed a dose-dependent increase [*Gdf15 and Hspa1b*] (Fig. 4B, Network-2). *Fos* and *Net1* in ENU-28 d-Network-3 showed a dose–response (Fig. 4B, Network-3). ENU-28 d-Network-4 (Table 2D) included different primary functions (cellular development, cellular growth, proliferation and connective tissue development and function) and 10 different genes from ENU-4 h-Network-4; two genes showed a dose–response [*Hspab1* and *Ung*]. ENU-28 d-Network-5 consisted of the same genes and the same top functions as those of DEN-4 h-Network-5, while no genes showed a dose–response in this study (Fig. 4A, Network-5).

4. Discussion

We examined the dose-dependency of gene expression changes for 51 genes in mouse liver treated with two *N*-nitroso genotoxic hepatocarcinogens, DEN and ENU, by qPCR at early times after administration. We selected 51 candidate genes based on our previous results of Affymetrix GeneChip Mu74AV2 and original DNA microarray of samples after treatment with DEN, dimethylnitrosamine, dipropylnitrosamine, ENU, *o*-aminoazotoluene, 7,12-dimethylbenz[*a*]anthracene, dibenzo[*a,l*]pyrene, phenobarbital and ethanol in our JEMS/MMS/Toxicogenomics group collaborative study. Because only a single dose was used for each chemical in the previous study, we examined dose-dependency in gene expression changes in this study using two representative chemicals. We showed distinct dose-dependency of gene expression changes induced by DEN and ENU; these changes associated with cancer, cell cycle arrest, DNA replication, recombination, repair and cell death not only at 4 h, but also, for some, at 28 days after administration. Similar gene expression changes between DEN and ENU were characteristic. Twenty-one genes exhibited a distinct dose-dependent increase at 4 h for both carcinogens [*Bax, Btg2, Ccng1, Cdkn1a, Cyp4a10, Cyp21a1, Fos, Gadd45b, Gdf15, Hmox1, Hspb1, Isg20l1, Jun, Mbd1, Mdm2, Myc, Net1, Plk2, Ppp1r3c, Rcan1* and *Tubb2c*], although the gene expression changed after ENU was generally weaker relative to that after DEN. The results were consistent with a previous report that showed more DNA lesions with DEN than with ENU a few hours after administration [6]. Only *Gdf15* showed a dose-dependent increase at 28 days for

both carcinogens. An additional seven different genes for DEN and eight genes for ENU also showed dose-dependency. *Ccng2*, *Hspb2*, *Igfbp1*, *Pmm1* and *Rad52* showed a dose-dependent increase and *Cyp1a2* and *Glul* showed a dose-dependent decrease 4 h after administration only with DEN. *Btg2*, *Cdkn1a* and *Cyp21a1* showed a dose-dependent increase 28 days after administration only with DEN and these genes also showed a dose–response at 4 h. *Ccnf*, *Fabp5* and *Hist1h1c* showed a dose-dependent increase 4 h after administration only with ENU. *Casp1*, *Fos*, *Gstk1*, *Hspa1b*, *Hspb2* and *Ung* showed a dose-dependent increase 28 days after administration only with ENU. *Ccnf* in DEN-4 h and *Bax* and *Ephx1* in DEN-28 d showed equivocal changes. We only observed several dose-dependent decreases in expression of genes [*Cyp1a2*, *Glul*, *Igfbp1* and *Net1*] after DEN and ENU in the present experimental conditions.

In the previous study [10], gene expression changes in number and degree were observed to peak at 4 h after administration and were lower at 20 h, 14 and 28 days. In the present study, we investigated the gene expression pattern at two different time points: 4 h, during production of many DNA lesions, and 28 days, during fixing of mutations [6]. We expected to observe the earliest and most varied effects in many cells in the liver, including DNA lesions, 4 h after administration. It was presumed that most of the DNA-damaged cells would be repaired, that some of the damaged cells would die and that only a few cells would progress to carcinogenesis. We reasoned that it would be useful to examine the earliest various effects to understand the potential gene-altering ability of carcinogens. The second time point, 28 days, is the time by which most mutations are fixed, the remainder of which would be related to carcinogenesis. We expected to observe gene expression changes which would reflect the effects of mutation at 28 days. The role of genes with altered expression might be different even if expression of the same gene was changed at 4 h and 28 days.

In addition, we examined gene networks using IPA to clarify interactions between genes with altered expression. IPA identified five networks of genes regulated at 4 h after DEN and ENU treatment (Table 3 and Fig. 4). As for DEN, 11 dose-dependent genes [*Bax*, *Btg2*, *Ccng1*, *Cdkn1a*, *Gadd45b*, *Gdf15*, *Hspb1*, *Hspb2*, *Mdm2*, *Plk2* and *Pmm1*] belonged to Network-1 (cancer and cell cycle) and the other 11 dose-dependent genes [*Ccng2*, *Cyp1a2*, *Cyp4a10*, *Cyp21a1*, *Gdf15*, *Glul*, *Igfbp1*, *Ppp1r3c Rad52*, *Rcan1* and *Tubb2c*] belonged to Network-2 (cell cycle, cell death, DNA replication, recombination and repair). In detail, *Gdf15* was extracted in both Network-1 and Network-2. As for ENU, 10 dose-dependent genes [*Bax*, *Btg2*, *Ccng1*, *Cdkn1a*, *Gadd45b*, *Gdf15*, *Hist1h1c*, *Hspb1*, *Mdm2* and *Plk2*] belonged to the same Network-1 and 7 dose-dependent genes [*Cyp21a1*, *Cyp4a10*, *Fabp5*, *Gdf15*, *Ppp1r3c*, *Rcan1* and *Tubb2c*] belonged to a different Network-2 (DNA replication, recombination and repair, and cell cycle and cell signaling). *Hspb2* and *Pmm1* showed dose–responses only in DEN-4 h-Network-1 and *Hist1h1c* showed a dose–response only in ENU-4 h-Network-1. [Cell death] in DEN-4 h-Network-2 was replaced with [Cell signaling] in ENU-4 h-Network-2. *Ccng2*, *Cyp1a2*, *Glul*, *Igfbp1* and *Rad52* showed dose–responses only in DEN-4 h-Network-2 and *Fabp5* showed a dose–response only in ENU-4 h-Network-2. This difference in Network-2 was the most remarkable difference between the effects of DEN and ENU in the present study. The top functions of Network-1 and Network-2 were characteristic networks for DEN-4 h and ENU-4 h, being typical of carcinogenic compounds. As for 28 days, IPA also identified five networks of genes, however, only a few genes showed a dose–response with DEN and ENU. As for DEN, three dose-dependent genes [*Btg2*, *Cdkn1a* and *Gdf15*] belonged to Network-1 and two genes [*Cyp21a1* and *Gdf15*] belonged to Network-2. As for ENU, three dose-dependent genes [*Casp1*, *Gdf15* and *Hspb2*] belonged to Network-1, [*Gdf15* and *Hspa1b*] belonged to Network-2, [*Fos* and *Net1*] belonged to Network-3 and [*Hspa1b* and *Ung*] belonged to Network-4. The present results suggested similar functions for *N*-nitroso carcinogens DEN and ENU, with several differences. We have examined effects of other genotoxic and non-genotoxic carcinogens in mouse liver at 4 h and have generated various networks for various carcinogens (unpublished).

We showed that Network-1 was associated with cancer and the cell cycle. To understand more detailed functions, we examined a major canonical pathway for each network. A major canonical pathway in Network-1 was *p53* signaling. The increase of *Cdkn1a*, *Ccng1* and *Gadd45* demonstrated cell cycle arrest. The expression pattern (Fig. 4) at 4 h showed that cell cycle arrest would proceed, to then be released by day 28. Both *p53* and *Bax* were associated with initiation of apoptosis.

In the same way, a major canonical pathway in Network-2 was aryl hydrocarbon receptor signaling [14]. Furthermore, aryl hydrocarbon receptor signaling as an adaptive response was manifested as the induction of xenobiotic metabolizing enzymes; *Cyp1a2*, *Cyp21a1* and *Cyp4a10* take part in this pathway. *Cyp21a1* also takes part in biosyntheses of steroid hormones [15]. Inflammation of the liver is controlled at 28 days after administration because steroid hormones function to suppress inflammation.

Growth/differentiation factor-15 (*Gdf15*) was the only gene whose expression increased at 4 h and 28 days of both DEN and ENU and belonged to Network-1 and Network-2 at 4 h and 28 days of DEN and ENU. *Gdf15* is a divergent Tgf-beta family member that is expressed following liver injury and carcinogen exposure [16]. *Gdf15* in liver is rapidly and dramatically up-regulated following various surgical and chemical treatments that cause acute liver injury and regeneration [17].

A major canonical pathway in Network-3 was platelet-derived growth factor (*Pdgf*) signaling. *Pdgfb*, *Kras*, *Jun*, *Fos* and *Myc* may be associated with *Pdgf* signaling. In this canonical pathway, *Pdgfb* phosphorylates other proteins and activates the downstream genes *Kras*, *Jun*, *Fos* and *Myc* [18–21], one reason why *Pdgfb* expression did not change significantly (Fig. 3A, Cluster-4).

Our results show that most differentially expressed genes at 4 h and 28 days exhibited a dose–response. Only a few genes, *Dpyd*, *Egfr*, *Lrp1* and *Ung* for DEN at 4 h; *Gyk* for ENU at 4 h; and *Ccng2* for ENU at 28 days showed atypical gene expression changes at the highest dose. These changes may be toxicity-related. *Dpyd* is associated with pyrimidine metabolism. *Egfr* is associated with cell proliferation. *Lrp* plays a clear protective role in atherogenesis. *Ung* is associated with DNA repair. Their decrease may show the loss of cell maintenance because hepatocytes will have received much lethal damage at the highest dose. *Gyk* is associated with xenobiotic metabolism signaling. It has been reported that glycerol kinase deficiency is involved in lipid metabolism, carbohydrate metabolism, and insulin signaling [22]. Indeed, it has been reported that type 2 diabetes is caused by ENU but not by DEN [23]. Unlike classical cyclins that promote cell cycle progression, cyclin G2 blocks cell cycle entry. The decrease of *Ccng2* mRNA may promote cell cycle progression.

Previously, we reported differential gene expression induced by two *N*-nitroso genotoxic hepatocarcinogens, DEN and dipropylnitrosamine (DPN) as compared to phenobarbital and ethanol in mouse liver examined with an original oligonucleotide microarray and qPCR [10]. We observed 11 differentially expressed genes 4 h after administration, including 7 tumor suppressor *Trp53* target genes, *Bax*, *Ccng1*, *Cdkn1a*, *Hspb2*/*Hsp27*, *Jun*, *Mdm2*, and *Plk2*/*Snk*; the other genes were *Ccnf*, *Hmox1*, *Mbd1*, and *Rad52*. Furthermore, some degree of differential gene expression of *Ccng1*, *Cdkn1a* and *Plk2*/*Snk* was observed 28 days after administration. In the present study, we selected 51 candidate genes (Table 1) based on our original DNA microarray and Affymetrix GeneChip Mu74AV2 data (not published) on seven genotoxic carcinogens, phenobarbital and ethanol. The present results show that 28 genes for

DEN and 29 genes for ENU exhibited dose-dependent differential expression. Differential gene expression was observed commonly at least for *Bax*, *Ccng1*, *Cdkn1a*, *Hmox1*, *Jun*, *Mbd1*, *Mdm2* and *Plk2* with these three *N*-nitroso carcinogens (DEN, DPN and ENU). As we expanded qPCR analysis from 14 genes in the previous study [10] to 51 genes in the present study, we could show complex gene networks by IPA. Twenty genes, *Btg2*, *Casp1*, *Ccng2*, *Cyp4a10*, *Cyp21a1*, *Ephx1*, *Gadd45b*, *Gdf15*, *Glul*, *Gstk1*, *Hspa1b*, *Hspb1*, *Igfbp1*, *Isg20l1*, *Net1*, *Pmm1*, *Ppp1r3c*, *Rcan1*, *Tubb2c* and *Ung*, which showed dose–responses in the present study, were newly examined.

We examined only pooled materials from five mice in the present study. However, we already reported that at least five genes (*Gapdh*, *Jun*, *Ccng1*, *Hspb2/Hsp27* and *Rad52*) exhibited only small inter-individual mouse gene expression variation [10] with DEN treatment after 4 h and 28 days. Additional study showed that *Bax*, *Hmox1*, *Mbd1*, *Mdm2* and *Plk2* also exhibited only small inter-individual gene expression variation with DEN treatment at 4 h and 28 days (unpublished data).

We will continue further studies on other types of chemicals for characterizing mutagenic and carcinogenic compounds; these data will be useful for chemical risk assessment and for furthering our understanding of the underlying biological processes.

Conflict of interest

We have not any conflicting interest include employment, consultancies, stock ownership, honoraria, paid expert testimony, patent applications/registrations, and grants or other funding.

Acknowledgements

This work was partly supported by KAKENHI (18310047) (C. Furihata, T. Watanabe and T. Suzuki), The Ministry of Education, Culture, Sports, Science and Technology, Japan and a High-Tech Research Center project for private universities with a matching fund subsidy from The Ministry of Education, Culture, Sports, Science and Technology, Japan (C. Furihata).

References

[1] B.A. Diwan, H. Meier, Carcinogenic effects of a single dose of diethylnitrosamine in three unrelated strains of mice: genetic dependence of the induced tumor types and incidence, Cancer Lett. 1 (1976) 249–253.
[2] A.P. Kyriazis, S.D. Vesselinovitch, Transplantability and biological behavior of mouse liver tumors induced by ethylnitrosourea, Cancer Res. 33 (1973) 332–338.
[3] J.A. Swenberg, M.C. Dyroff, M.A. Bedell, J.A. Popp, N. Huh, U. Kirstein, M.F. Rajewsky, O4-ethyldeoxythymidine, but not O6-ethyldeoxyguanosine, accumulates in hepatocyte DNA of rats exposed continuously to diethylnitrosamine, Proc. Natl. Acad. Sci. U.S.A. 81 (1984) 1692–1695.
[4] J.L. Yang, P.C. Lee, S.R. Lin, J.G. Lin, Comparison of mutation spectra induced by N-ethyl-N-nitrosourea in the hprt gene of Mer+ and Mer− diploid human fibroblasts, Carcinogenesis 15 (1994) 939–945.
[5] T. Suzuki, M. Hayashi, T. Sofuni, Initial experiences and future directions for transgenic mouse mutation assays, Mutat. Res. 307 (1994) 489–494.
[6] E.J. Mientjes, A. Luiten-Schuite, E. van der Wolf, Y. Borsboom, A. Bergmans, F. Berends, P.H. Lohman, R.A. Baan, J.H. van Delft, DNA adducts, mutant frequencies, and mutation spectra in various organs of lambda lacZ mice exposed to ethylating agents, Environ. Mol. Mutagen. 31 (1998) 18–31.
[7] J.F. Waring, R.A. Jolly, R. Ciurlionis, P.Y. Lum, J.T. Praestgaard, D.C. Morfitt, B. Buratto, C. Roberts, E. Schadt, R.G. Ulrich, Clustering of hepatotoxins based on mechanism of toxicity using gene expression profiles, Toxicol. Appl. Pharmacol. 175 (2001) 28–42.
[8] M.J. Bartosiewicz, D. Jenkins, S. Penn, J. Emery, A. Buckpitt, Unique gene expression patterns in liver and kidney associated with exposure to chemical toxicants, J. Pharmacol. Exp. Ther. 297 (2001) 895–905.
[9] M. Provenzano, S. Mocellin, Complementary techniques: validation of gene expression data by quantitative real time PCR, Adv. Exp. Med. Biol. 593 (2007) 66–73.
[10] T. Watanabe, K. Tobe, Y. Nakachi, Y. Kondoh, M. Nakajima, S. Hamada, C. Namiki, T. Suzuki, S. Maeda, A. Tadakuma, M. Sakurai, Y. Arai, A. Hyogo, M. Hoshino, T. Tashiro, H. Ito, H. Inazumi, Y. Sakaki, H. Tashiro, C. Furihata, Differential gene expression induced by two genotoxic *N*-nitroso carcinogens, phenobarbital and ethanol in mouse liver examined with oligonucleotide microarray and quantitative real-time PCR, Gene Environ. 29 (2007) 115–127.
[11] K. Sekihashi, A. Yamamoto, Y. Matsumura, S. Ueno, M. Watanabe-Akanuma, F. Kassie, S. Knasmüller, S. Tsuda, Y.F. Sasaki, Comparative investigation of multiple organs of mice and rats in the comet assay, Mutat. Res. 517 (2002) 53–75.
[12] S. Madle, S.W. Dean, U. Andrae, G. Brambilla, B. Burlinson, D.J. Doolittle, C. Furihata, T. Hertner, C.A. McQueen, H. Mori, Recommendations for the performance of UDS tests in vitro and in vivo, Mutat. Res. 312 (1994) 263–285.
[13] A. Sturn, J. Quackenbush, Z. Trajanoski, Genesis: Cluster analysis of microarray data, Bioinformatics 18 (2002) 207–208.
[14] D.W. Kim, L. Gazourian, S.A. Quadri, R. Romieu-Mourez, D.H. Sherr, G.E. Sonenshein, The RelA NF-kappaB subunit and the aryl hydrocarbon receptor (AhR) cooperate to transactivate the Myc promoter in mammary cells, Oncogene 19 (2000) 5498–5506.
[15] J. Gonçalves, A. Friães, L. Moura, Congenital adrenal hyperplasia: focus on the molecular basis of 21-hydroxylase deficiency, Expert Rev. Mol. Med. 9 (2007) 1–23.
[16] T.A. Zimmers, X. Jin, J.C. Gutierrez, C. Acosta, I.H. McKillop, R.H. Pierce, L.G. Koniaris, Effect of in vivo loss of GDF-15 on hepatocellular carcinogenesis, J. Cancer Res. Clin. Oncol. 134 (2008) 753–759.
[17] E.C. Hsiao, L.G. Koniaris, T. Zimmers-Koniaris, S.M. Sebald, T.V. Huynh, S.J. Lee, Characterization of growth-differentiation factor 15, a transforming growth factor beta superfamily member induced following liver injury, Mol. Cell. Biol. 20 (2000) 3742–3751.
[18] S. Svegliati, R. Cancello, P. Sambo, M. Luchetti, P. Paroncini, G. Orlandini, G. Discepoli, R. Paterno, M. Santillo, C. Cuozzo, S. Cassano, E.V. Avvedimento, A. Gabrielli, Platelet-derived growth factor and reactive oxygen species (ROS) regulate Ras protein levels in primary human fibroblasts via ERK1/2. Amplification of ROS and Ras in systemic sclerosis fibroblasts, J. Biol. Chem. 280 (2005) 36474–36482.
[19] J.W. Tullai, M.E. Schaffer, S. Mullenbrock, S. Kasif, G.M. Cooper, Identification of transcription factor binding sites upstream of human genes regulated by the phosphatidylinositol 3-kinase and MEK/ERK signaling pathways, J. Biol. Chem. 279 (2004) 20167–20177.
[20] A.J. Kudla, M.L. John, D.F. Bowen-Pope, B. Rainish, B.B. Olwin, A requirement for fibroblast growth factor in regulation of skeletal muscle growth and differentiation cannot be replaced by activation of platelet-derived growth factor signaling pathways, Mol. Cell. Biol. 15 (1995) 3238–3246.
[21] P.A. Bromann, H. Korkaya, C.P. Webb, J. Miller, T.L. Calvin, S.A. Courtneidge, Platelet-derived growth factor stimulates Src-dependent mRNA stabilization of specific early genes in fibroblasts, J. Biol. Chem. 280 (2005) 10253–10263.
[22] L. Rahib, N.K. MacLennan, S. Horvath, J.C. Liao, K.M. Dipple, Glycerol kinase deficiency alters expression of genes involved in lipid metabolism, carbohydrate metabolism, and insulin signaling, Eur. J. Hum. Genet. 15 (2007) 646–657.
[23] A.A. Toye, L. Moir, A. Hugill, L. Bentley, J. Quarterman, V. Mijat, T. Hough, M. Goldsworthy, A. Haynes, A.J. Hunter, M. Browne, N. Spurr, R.D. Cox, A new mouse model of type 2 diabetes, produced by N-ethyl-nitrosourea mutagenesis, is the result of a missense mutation in the glucokinase gene, Diabetes 53 (2004) 1577–1583.

Cell

Estrogen Prevents Bone Loss via Estrogen Receptor α and Induction of Fas Ligand in Osteoclasts

Takashi Nakamura,[1,2,9] Yuuki Imai,[1,3,9] Takahiro Matsumoto,[1,2] Shingo Sato,[4] Kazusane Takeuchi,[1] Katsuhide Igarashi,[5] Yoshifumi Harada,[6] Yoshiaki Azuma,[6] Andree Krust,[7] Yoko Yamamoto,[1] Hiroshi Nishina,[4] Shu Takeda,[4] Hiroshi Takayanagi,[4] Daniel Metzger,[7] Jun Kanno,[5] Kunio Takaoka,[3] T. John Martin,[8] Pierre Chambon,[7] and Shigeaki Kato[1,2,*]

[1]Institute of Molecular and Cellular Biosciences, University of Tokyo, Yayoi 1-1-1, Bunkyo-ku, Tokyo 113-0032, Japan

[2]Exploratory Research for Advanced Technology, Japan Science and Technology Agency, Honcho 4-1-8, Kawaguchi, Saitama 332-0012, Japan

[3]Department of Orthopaedic Surgery, Osaka City University Graduate School of Medicine, Asahimachi 1-4-3, Abeno-ku, Osaka, 545-8585, Japan

[4]Tokyo Medical and Dental University, Yushima 1-5-45, Bunkyo-ku, Tokyo 113-8510, Japan

[5]Division of Cellular and Molecular Toxicology, National Institute of Health Sciences, 1-18-1 Kamiyoga, Setagaya-ku, Tokyo 158-8501, Japan

[6]Teijin Institute for Biomedical Research, Asahigaoka 4-3-2, Hino, Tokyo 191-8512, Japan

[7]Institut de Génétique et de Biologie Moleculaire et Cellulaire, Departement of Physiological Genetics / Inserm, U-596 / CNRS, UMR7104 / Université Louis Pasteur, Illkirch, Strasbourg, F-67400 France

[8]St. Vincent's Institute of Medical Research, 9 Princes Street, Fitzroy VIC 3065, Australia

[9]These authors contributed equally to this work.

*Correspondence: uskato@mail.ecc.u-tokyo.ac.jp

DOI 10.1016/j.cell.2007.07.025

SUMMARY

Estrogen prevents osteoporotic bone loss by attenuating bone resorption; however, the molecular basis for this is unknown. Here, we report a critical role for the osteoclastic estrogen receptor α (ERα) in mediating estrogen-dependent bone maintenance in female mice. We selectively ablated ERα in differentiated osteoclasts ($ER\alpha^{\Delta Oc/\Delta Oc}$) and found that $ER\alpha^{\Delta Oc/\Delta Oc}$ females, but not males, exhibited trabecular bone loss, similar to the osteoporotic bone phenotype in postmenopausal women. Further, we show that estrogen induced apoptosis and upregulation of Fas ligand (FasL) expression in osteoclasts of the trabecular bones of WT but not $ER\alpha^{\Delta Oc/\Delta Oc}$ mice. The expression of ERα was also required for the induction of apoptosis by tamoxifen and estrogen in cultured osteoclasts. Our results support a model in which estrogen regulates the life span of mature osteoclasts via the induction of the Fas/FasL system, thereby providing an explanation for the osteoprotective function of estrogen as well as SERMs.

INTRODUCTION

Bone remodeling is a dynamic metabolic process. The destruction or "resorption" of pre-existing bone by mature osteoclasts is followed by the formation of new bone by osteoblasts. Osteoblasts are derived from pleiotropic mesenchymal stem cells in the bone marrow. Mature osteoclasts are multinuclear, macrophage-like cells, derived from hematopoietic stem cells also in the bone marrow. Bone resorption and deposition are tightly coupled, and their balance defines both bone mass as well as quality. The regulation of bone remodeling is complex. A number of systemic hormones and transcription factors directly regulate the proliferation and differentiation of osteoblasts and osteoclasts (Karsenty, 2006; Karsenty and Wagner, 2002; Rodan and Martin, 2000; Teitelbaum and Ross, 2003). Additionally, the indirect cellular communication among groups of bone cells is also physiologically critical for bone growth and remodeling (Martin and Sims, 2005; Mundy and Elefteriou, 2006). The molecular and genetic mechanisms governing bone cell fate have been intensively studied; however, how the life span of bone cells is determined on a molecular level remains elusive.

Estrogen is a key hormone in bone remodeling in several species. The osteoprotective action of estrogen is demonstrable in rodents and is clinically important in humans, particularly older women (Chien and Karsenty, 2005;

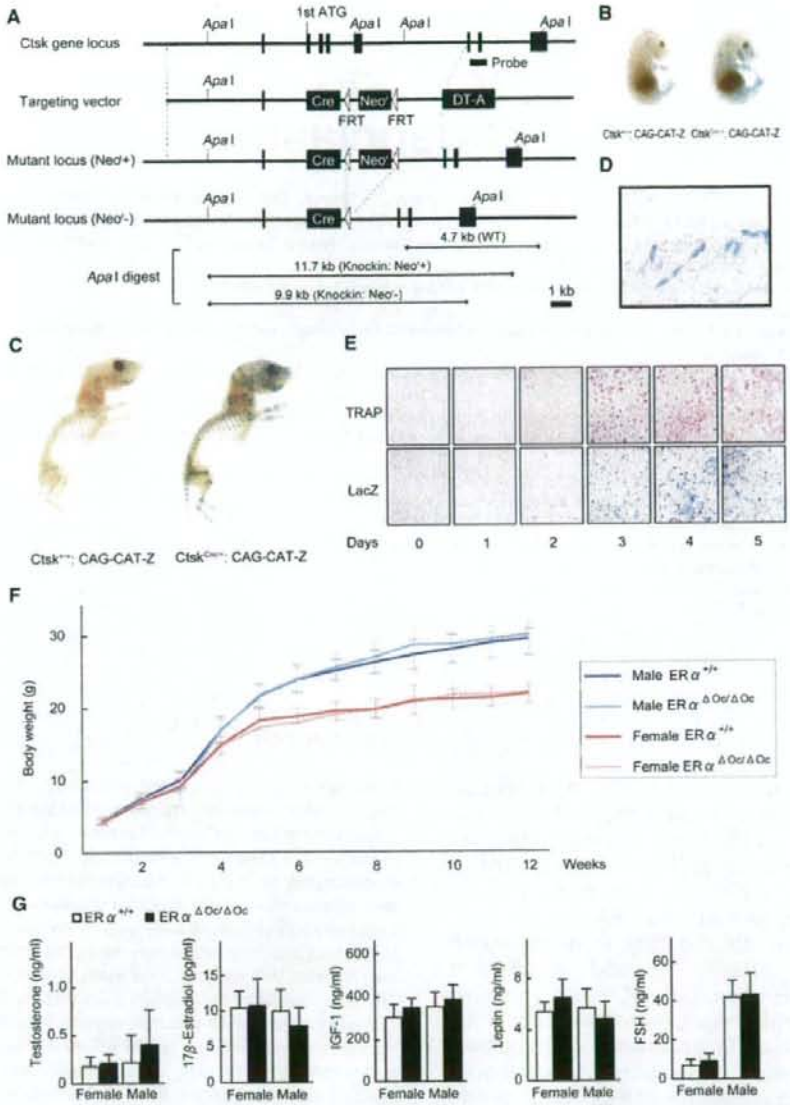

Figure 1. Generation of Knockin Mice Selectively Expressing Cre in Mature Osteoclasts

(A) Illustration of the targeting strategy for insertion of the *Cre* gene into the mouse *Cathepsin K* (*Ctsk*) gene. A targeting vector was generated to contain the *Cre* cDNA at the endogenous ATG start site, followed by a *FRT* (Flp-recombinase target)-flanked *Neo*^{r} cassette. The *DT-A* (diphtheria toxin-A) gene was also inserted to avoid random integrations.

(B and C) *Ctsk-Cre* mice were then crossed with *CAG-CAT-Z* mice. β-galactosidase activity derived from the activated *LacZ* reporter gene was monitored to test if expressed Cre excised the *loxP* sites in mature osteoclasts. LacZ expression patterns reflected the localization patterns of mature osteoclasts in the developing bone at 16.5 days post coitum embryos and in the skeletal tissues of 7-day-old pups.

(D) The LacZ expression induced by Cre-mediated excision was also seen in osteoclasts attached to trabecular bone in the lumber vertebrae of 12-week-old mice.

(E) LacZ expression was induced during osteoclastogenesis. Osteoclast-like cells that differentiated from bone-marrow macrophages following culture in the presence of M-CSF and RANKL were stained with TRAP (tartrate-resistant acid phosphatase), a mature osteoclast marker.

Delmas, 2002; Raisz, 2005; Rodan and Martin, 2000). Estrogen deficiency in postmenopausal women frequently leads to osteoporosis, the most common skeletal disorder. Similarly, ovariectomy clearly produces an osteoporotic bone phenotype in mice. Osteoporotic bone loss is the result of high bone turnover in which bone resorption outpaces bone deposition (Rodan and Martin, 2000; Teitelbaum, 2007). This imbalance in bone turnover that is induced by estrogen deficiency in women and female rodents can be ameliorated with bio-available estrogens including selective estrogen receptor modulators (SERMs) (Riggs and Hartmann, 2003).

Estrogen and SERMs primarily act by regulating gene transcription via estrogen receptors (ERα, ERβ) (Couse and Korach, 1999; Shang and Brown, 2002). ERs belong to the nuclear receptor gene superfamily and act as ligand-inducible transcriptional factors (Mangelsdorf et al., 1995). ER dimers directly or indirectly associate with specific DNA elements in the target gene promoter (Shang and Brown, 2002) and control transcription through reorganizing chromatin structure and histone modifications (Belandia and Parker, 2003). Genetic mouse models (KO mice) lacking ERα ($ER\alpha^{-/-}$) and ERβ ($ER\beta^{-/-}$) provide insights into ER function (Mueller and Korach, 2001; Windahl et al., 2002). In mice, though ERα appears to be the major receptor in most estrogen target tissues including bone (Sims et al., 2003), neither clear bone loss nor high bone turnover is detectable in ERα single or ERα/ERβ double-KO females (Syed and Khosla, 2005; Windahl et al., 2002). This unexpected maintenance of bone mass in female mutants is presumed to be due to unphysiologically elevated levels of other osteoprotective hormones, like androgens. Systemic defects in the hypothalamus caused by ER inactivation appear to impair the negative feedback system of hormone production (Syed and Khosla, 2005). This leads to an excess in estrogen precursors, notably androgens. In fact, the anabolic effects of androgens mediated by the androgen receptor (AR) are evident in female mice (Kawano et al., 2003; Sims et al., 2003). In males, estrogen is also osteoprotective, as is evident by the development of osteopenia in male patients genetically deficient in ERα (Smith et al., 1994) or aromatase activity (Simpson and Davis, 2001). Thus, irrespective of the accumulating clinical and basic research data on the osteoprotective actions of estrogen and SERMs, the molecular basis of this osteoprotection in females remains elusive.

To study the molecular interactions behind the antibone resorptive actions of estrogen in women and female animals, we genetically ablated ERα in mature osteoclasts ($ER\alpha^{\Delta Oc/\Delta Oc}$). Selective ablation of ERα in differentiated osteoclasts ($ER\alpha^{\Delta Oc/\Delta Oc}$) was accomplished by crossing a *Cathepsin K-Cre* knockin mouse with a floxed *ERα* mouse. This resulted in clear trabecular bone loss and high bone turnover associated with increased osteoclast numbers in females but not in males. In the female mutants, further bone loss following ovariectomy was not significant and recovery by estrogen was ineffective in the trabecular areas of long bones and lumbar vertebral bodies. Upregulated expression of *Fas ligand* (*FasL*) gene, and increased apoptosis in differentiated osteoclasts by estrogen was found in the intact bone of wild-type females but undetectable in $ER\alpha^{\Delta Oc/\Delta Oc}$ females. Induction of FasL and apoptosis by estrogen as well as a SERM also required ERα in cultured osteoclasts. Thus, we propose that the osteoprotective actions of estrogen and SERMs are mediated at least in part through osteoclastic ERα in trabecular bone, and the life span of mature osteoclasts is regulated through the activation of the FasL signaling.

RESULTS

Generation of Osteoclast-Specific *ERα* Gene Disruption by Knocked-In *Cre* in the *Cathepsin K* Gene

To specifically disrupt *ERα* gene in mature osteoclasts, we knocked in *Cre* into the gene locus of *Cathepsin K* ($Ctsk^{Cre/+}$) (Figures 1A, S1A, and S1B), a gene known to be expressed in differentiated osteoclastic cells arising from hematopoietic stem cells. This gene is functionally indispensable for mature osteoclasts (Saftig et al., 1998). Only one copy appears enough to support normal bone formation and bone turnover, since heterozygous mutant mice of *Cathepsin K* ($Ctsk^{+/-}$) have no obvious bone phenotype (Gowen et al., 1999; Li et al., 2006; Saftig et al., 1998) . Clear, bone-specific expression of the *Cre* transcript in the adult $Ctsk^{Cre/+}$ mice was observed in the tested tissues (Figure S1C). To confirm Cre protein expression, the $Ctsk^{Cre/+}$ mice were crossed with tester mice (*CAG-CAT-Z*). These mice were genetically engineered to express β-galactosidase by excision of the transcribed stop sequence in front of the *β-galactosidase* gene (*LacZ*) in cells expressing Cre (Sakai and Miyazaki, 1997). β-galactosidase expression visualized by LacZ staining was observed in the bones of 16.5 dpc embryos and 7-day-old pups of $Ctsk^{Cre/+}$; *CAG-CAT-Z* mice. Expression patterns were consistent with the appearance and skeletal localization of functionally mature osteoclasts (Figures 1B and 1C). Histochemical staining of LacZ in the lumbar vertebrae of 12-week-old mice was localized in multinuclear osteoclasts (Figure 1D) but not seen in osteoblasts and osteocytes (Figure S1D) and the hypothalamus (Figure S1E). Since *Cathepsin K* gene expression is evident in differentiated osteoclasts (Saftig et al., 1998), we used an in vitro culture cell system to test whether Cre expression was driven by the endogenous promoter that is induced at the time of osteoclast differentiation. Osteoclast-precursor cells derived from bone marrow

(F) The growth curve of $ER\alpha^{\Delta Oc/\Delta Oc}$ mice was indistinguishable from that of the control mice. Data are represented as mean ± SEM.
(G) Serum hormone levels were normal in 12-week-old $ER\alpha^{\Delta Oc/\Delta Oc}$ (filled column) versus $ER\alpha^{+/+}$ (open column) mice (n = 10–11 animals per genotype). Data are represented as mean ± SEM.

were cytodifferentiated for 1 week in the presence of M-CSF (macrophage colony stimulating factor) and RANKL (receptor activator of NFκB ligand) (Koga et al., 2004). TRAP-positive osteoclasts emerged after 3 days of culture (Figure 1E). The number of TRAP-positive osteoclasts and the number of LacZ-expressing cells simultaneously increased. In the contrast, the LacZ expression was not detected in primary cultured osteoblasts derived from the calvaria (Figure S1F). In view of both our in vivo and in vitro observations, we conclude that the *Ctsk*$^{Cre/+}$ mouse line expresses Cre in differentiated osteoclasts. Moreover, estrogen response in bone mass control was not distinguishable in between *Ctsk*$^{Cre/+}$ and *Ctsk*$^{+/+}$ mice (Figure S2A).

We then crossed floxed *ER*α mice (Dupont et al., 2000) with *Ctsk*$^{Cre/+}$ mice to disrupt ERα in differentiated osteoclasts (*ER*α$^{\Delta Oc/\Delta Oc}$). Excision of the *ER*α gene (Figure S1G) was confirmed by Southern blotting of DNA from adult female and male (data not shown) bone as well as in cultured mature osteoclasts (Figure S1H). No overt differences were observed in the growth curve, reproduction, or tissues for up to 12 weeks of age (Figure 1F) between the *Ctsk*$^{Cre/+}$; *ER*α$^{+/+}$ (*ER*α$^{+/+}$) and the *Ctsk*$^{Cre/+}$; *ER*α$^{flox/flox}$ (*ER*α$^{\Delta Oc/\Delta Oc}$) mice, with the exception of the female bones. Serum levels of sex hormones and bone remodeling regulators such as IGF-I, leptin, and follicle-stimulating hormone (Sun et al., 2006; Takeda et al., 2002) appeared unchanged in both male and female *ER*α$^{\Delta Oc/\Delta Oc}$ mice at 12 weeks (Figure 1G).

Osteopenia Occurred in Osteoclast-Specific ERα KO Females But Not Males

The 12-week-old *ER*α$^{\Delta Oc/\Delta Oc}$ females exhibited a clear reduction in bone mineral density (BMD) in the femurs (Figures 2A–2C) and tibiae (data not shown) when compared with *ER*α$^{+/+}$ mice. Though cortical bone appeared unaffected, trabecular bone loss (Figure 2A) with significant reduction of trabecular bone volume (BV/TV) (Figure 2F) was clearly seen. This is similar to the osteoporotic abnormalities observed in women during natural menopause or following ovariectomy (Delmas, 2002; Tolar et al., 2004). However, unlike men deficient in aromatase or ERα activity (Simpson and Davis, 2001; Smith et al., 1994), *ER*α$^{\Delta Oc/\Delta Oc}$ males unexpectedly exhibited no clear bone loss even in the trabecular areas (Figures 2A–2C). In *ER*α$^{\Delta Oc/\Delta Oc}$ females, both the bone-formation rate, estimated by double-calcein labeling (Figure 2D), as well as the bone-resorption rate, estimated from TRAP-positive differentiated osteoclast numbers (Figure 2E), were increased, indicating high bone turnover. Histomorphometric analyses of *ER*α$^{\Delta Oc/\Delta Oc}$ females supported the observation of accelerated bone resorption, as increased numbers of osteoclasts (Oc. S/BS and N. Oc/BS) were observed together with more eroded bone surface (ES/BS in Figure 2F). Bone formation was also enhanced as the rates of mineral apposition (MAR) and bone formation (BFR/BS) were both upregulated without an increase in osteoblast numbers (Ob.S/BS) (Figure 2F). Thus, considering all of these findings, it is conceivable that the increased number of differentiated osteoclasts following ERα ablation accelerates bone resorption over formation, leading to bone loss in the trabecular areas.

No Further Bone Loss Results from Estrogen Deficiency in *ER*α$^{\Delta Oc/\Delta Oc}$ Females

To verify whether osteoclastic ERα indeed mediates osteoprotective estrogen actions, estrogen action was investigated by ovariectomy (OVX) of 12-week-old female mice. As expected, OVX in *ER*α$^{+/+}$ females resulted in significantly reduced BMD particularly in the trabecular bone (Figures 3A and 3B) but not in the cortical bone (Figure 3C). Consistent with previous reports, (Kimble et al., 1995; Teitelbaum and Ross, 2003), estrogen deficiency following OVX upregulated the serum levels of cytokines like TNFα and IL-1α (Figure 3D). These cytokines enhance bone resorption through stimulation of osteoclastogenesis, leading to the loss of bone mass (Teitelbaum and Ross, 2003). OVX did not further reduce BMD or trabecular bone volume of the femurs of *ER*α$^{\Delta Oc/\Delta Oc}$ females (Figure 3B) nor affect increased number of TRAP-positive osteoclasts (see lower panel in Figure 3A) despite upregulation of serum cytokines. This suggests that the expression of cytokines known to regulate bone resorption is not under the control of osteoclastic ERα.

Estrogen Treatment Failed to Rescue the Osteoporotic Bone Phenotype of *ER*α$^{\Delta Oc/\Delta Oc}$ Mice

Estrogen treatment by estrogen pellet implantation (OVX + E2) for 2 weeks after OVX in *ER*α$^{+/+}$ mice elicited a dramatic increase in bone mass in both the trabecular and cortical areas of the femurs (data not shown) and lumbar vertebral bodies (Figure 4A). Estrogen action during E2 treatment in female mutants (*ER*α$^{\Delta Oc/\Delta Oc}$) was not as pronounced as in the *ER*α$^{+/+}$ females (Figures 4A and 4B), and the increase in the trabecular portions of the distal femurs was slight (data not shown). Histomorphometric analysis of the lumbar vertebral bodies (Figure 4B) supported the idea that E2 treatment in the female mutants was not sufficient to suppress accelerated bone resorption. These in vivo findings in the *ER*α$^{\Delta Oc/\Delta Oc}$ females suggest that in at least the trabecular areas of the long bones and lumbar vertebral bodies, the osteoprotective estrogen action is primarily mediated via osteoclastic ERα inhibiting bone resorption.

To further test this hypothesis, we investigated ERα protein expression in mature osteoclasts from trabecular bone. Few reports document osteoclastic expression of ERα protein and an estrogen response in both intact animals and in in vitro cultured osteoclasts (Bland, 2000). We therefore reasoned that ER expression ceases during differentiation into mature cells from primary cultures of osteoclast precursors, similar to that observed in other primary culture cell systems such as avian oviduct cells, in which ERα protein expression is drastically decreased during culture (Kato et al., 1989). Using highly sensitive immunohistochemistry, we investigated whether

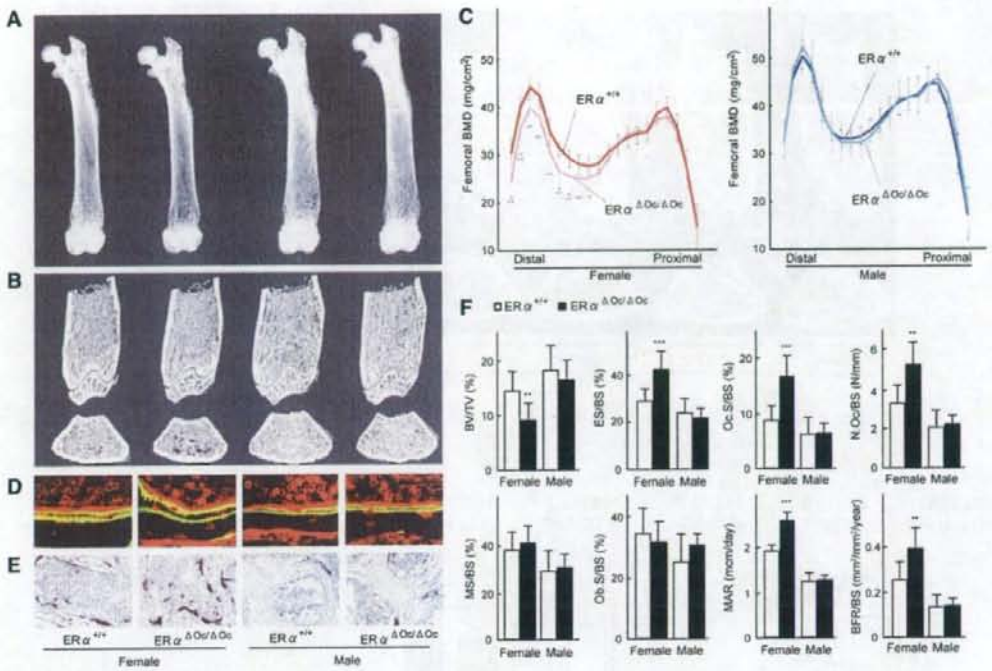

Figure 2. High Bone Turnover Osteopenia Was Observed in $ER\alpha^{\Delta Oc/\Delta Oc}$ Females But Not Males

(A) Soft X-ray images of femurs from 12-week-old $Ctsk^{Cre/+}$; $ER\alpha^{flox/flox}$ ($ER\alpha^{\Delta Oc/\Delta Oc}$) mice.

(B) Three-dimensional computed tomography images of the distal femurs and axial sections of distal metaphysis from representative 12-week-old $Ctsk^{Cre/+}$; $ER\alpha^{+/+}$ ($ER\alpha^{+/+}$) and $ER\alpha^{\Delta Oc/\Delta Oc}$ mice.

(C) BMD of each of 20 equal longitudinal divisions of femurs from 12-week-old $ER\alpha^{+/+}$ and $ER\alpha^{\Delta Oc/\Delta Oc}$ mice. (n = 10–11 animals per genotype; Student's t test, *p < 0.05; **p < 0.01; ***p < 0.001). Data are represented as mean ± SEM.

(D) Bone formation was also accelerated in $ER\alpha^{\Delta Oc/\Delta Oc}$ females when two calcein-labeled mineralized fronts visualized by fluorescent micrography were measured in the proximal tibia of 12-week-old mice.

(E) The number of TRAP-positive osteoclasts in the lumbar spine of female mice was increased by selective disruption of ERα in osteoclasts, indicating enhanced bone resorption.

(F) Bone turnover parameters as measured by dynamic bone histomorphometry after calcein labeling indicated high bone turnover in $ER\alpha^{\Delta Oc/\Delta Oc}$ females. Parameters are measured in the proximal tibia of 12-week-old $ER\alpha^{+/+}$ (open column) and $ER\alpha^{\Delta Oc/\Delta Oc}$ (filled column) mice. BV/TV: bone volume per tissue volume. ES/BS: eroded surface per bone surface. Oc.S/BS: osteoclast surface per bone surface. N.Oc/BS: osteoclast number per bone surface. MS/BS: mineralizing surface per bone surface. Ob.S/BS: osteoblast surface per bone surface. MAR: mineral apposition rate. BFR/BS: bone formation rate per bone surface (n = 10–11 animals per genotype; Student's t test, *p < 0.05; **p < 0.01; ***p < 0.001). Data are represented as mean ± SEM.

ERα protein expresses in differentiated osteoclasts in the bone tissues of femur sections from 12-week-old mice. ERα protein expression appeared abundant in osteoblasts and osteocytes of femur sections (Figure 4C) as well as hypothalamus (Figure S2B) from 12-week-old mice, in agreement with a previous report (Zaman et al., 2006). Likewise, expression levels of ERα in primary cultured osteoblasts derived from calvaria of $ER\alpha^{\Delta Oc/\Delta Oc}$ females appeared unaffected (Figure S2C). In contrast, in differentiated osteoclasts of the same femur sections, ERα expression was definitely detectable but very low in the $ER\alpha^{+/+}$ but undetectable in $ER\alpha^{\Delta Oc/\Delta Oc}$ females (Figure 4C).

Signaling by Osteoclastogenic Factors and Osteoclastogenesis Is Intact in Osteoclasts Deficient in ERα

It is possible that the osteoprotective function of osteoclastic ERα inhibits osteoclastogenesis. To address this issue, osteoclastogenesis was tested in cultured osteoclasts derived from bone-marrow cells of $ER\alpha^{\Delta Oc/\Delta Oc}$ mutants. In this cell culture system, a possible contribution of contaminated immune cells and stromal cells could be excluded, since osteoclastogenesis is only inducible by M-CSF treatment followed by M-CSF + RANKL (Koga et al., 2004).

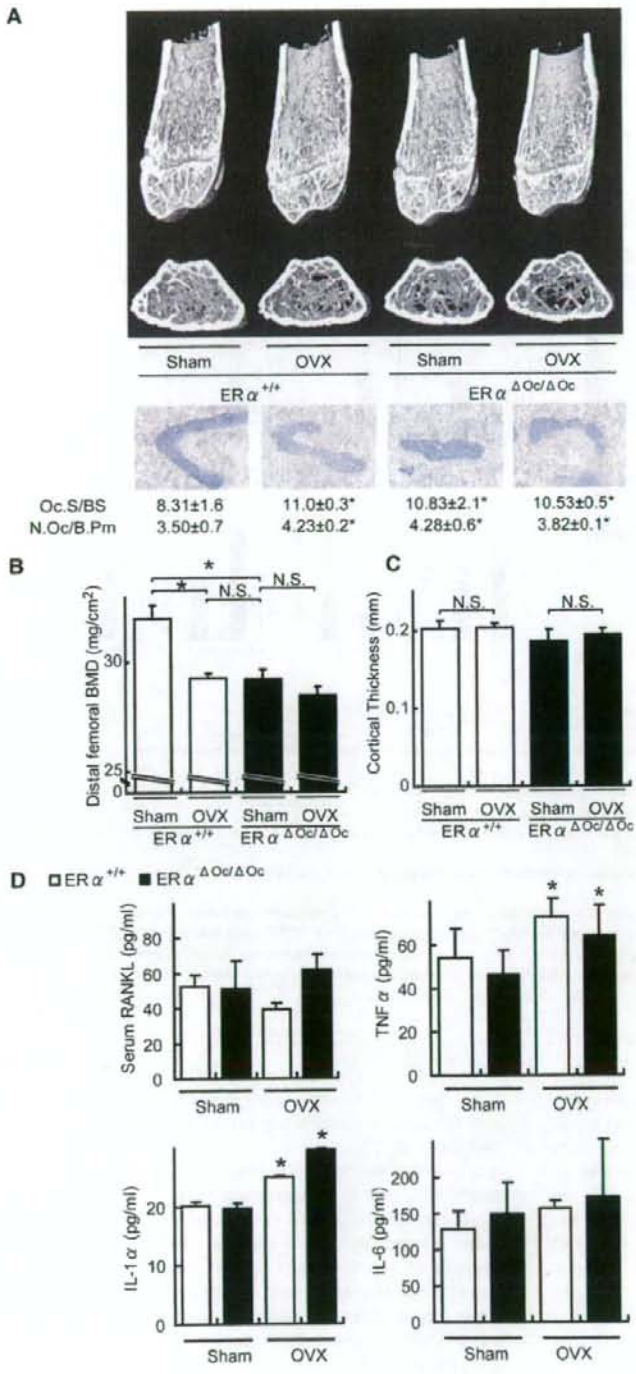

Figure 3. No Further Bone Loss of $ER\alpha^{\Delta Oc/\Delta Oc}$ Females by Ovariectomy

(A) Distal femoral micro CT analysis and lumbar vertebral bone histomorphometrical analysis of sham-operated or ovariectomized (OVX) 12-week-old $ER\alpha^{+/+}$ and $ER\alpha^{\Delta Oc/\Delta Oc}$ mice (*$p < 0.05$ compared to $ER\alpha^{+/+}$ sham group). Two weeks after OVX, the bone phenotype was analyzed.

(B) BMD of the distal femurs within each group are described in Figure 3A (*$p < 0.05$; N.S., not significant). Data are represented as mean ± SEM.

(C) Cortical thickness evaluation from micro CT analysis of femurs within each group described in Figure 3A. Data are represented as mean ± SEM.

(D) The levels of TNFα, IL-1α, and IL-6 in the bone-marrow cells culture media and serum RANKL (*$p < 0.05$ compared to each sham group). Data are represented as mean ± SEM.

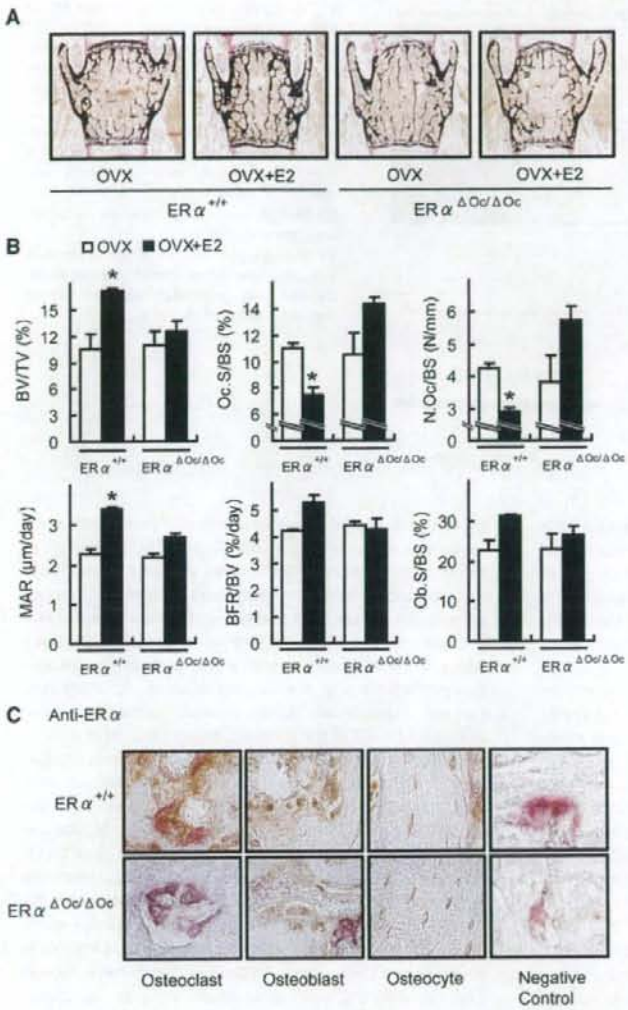

Figure 4. Estrogen treatment failed to reverse trabecular bone loss of ovariectomized $ER\alpha^{\Delta Oc/\Delta Oc}$ females

(A) von kossa staining of lumbar vertebral bodies of ovariectomized $ER\alpha^{+/+}$ and $ER\alpha^{\Delta Oc/\Delta Oc}$ mice treated with or without 17β-estradiol (0.83 μg/day) for 2 weeks (+E2) groups.

(B) Bone histomorphometrical analyses of the lumber vertebral bodies of 12-week-old ovariectomized $ER\alpha^{+/+}$ (left columns) and $ER\alpha^{\Delta Oc/\Delta Oc}$ (right columns) mice with (filled columns) or without (open columns) E2 treatment for 2 weeks (*$p < 0.05$ compared with E2-treated ovariectomized $ER\alpha^{\Delta Oc/\Delta Oc}$ mice). BV/TV: bone volume per tissue volume. ES/BS: eroded surface per bone surface. Oc.S/BS: osteoclast surface per bone surface. N.Oc/BS: osteoclast number per bone surface. MS/BS: mineralizing surface per bone surface. Ob.S/BS: osteoblast surface per bone surface. MAR: mineral apposition rate. BFR/BS: bone formation rate per bone surface. Data are represented as mean ± SEM.

(C) Immunochemical identification of ERα (brown) in TRAP-positive (red) differentiated osteoclasts. The femurs of 12 week-old mice were used for the immunodetection of ERα in bone cells. All labels were abolished when the primary antibody was preadsorbed with the immunizing peptide (negative control).

The number of TRAP-positive osteoclasts differentiated from the bone-marrow cells of $ER\alpha^{\Delta Oc/\Delta Oc}$ females was almost the same as that from $ER\alpha^{+/+}$ females (Figure 5A) and males (data not shown). The differentiated $ER\alpha^{\Delta Oc/\Delta Oc}$ osteoclasts had typical osteoclastic features, including the characteristic cell shape, TRAP-positive, multiple nuclei, and actin-ring formation, and were indistinguishable from the $ER\alpha^{+/+}$ osteoclasts (Figure 5B).

The expression levels of the prime osteoclastogenic transcription factors, *c-fos* and *NFATc1*, were unaltered by ERα deficiency in differentiated osteoclasts (Figure 5C). Furthermore, responses to RANKL in intracellular signaling, as represented by phosphorylation of p38 and IκB, were unaffected in $ER\alpha^{\Delta Oc/\Delta Oc}$ osteoclasts from females (Figure 5D) as well as males (data not shown). In light of these findings, it is unlikely that activated ERα in osteoclastic cells attenuates osteoclastogenesis.

Activation of the Fas/FasL System by Estrogen in Intact Bone Is Impaired by Osteoclastic ERα Deficiency

To examine osteoclastic ERα function in intact bone, DNA microarray analysis following real-time RT-PCR of RNA from the femurs of ovariectomized $ER\alpha^{\Delta Oc/\Delta Oc}$ females treated with or without estrogen, was performed. During

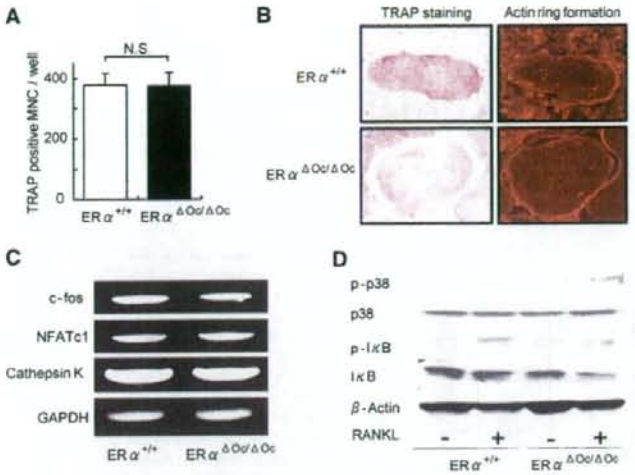

Figure 5. ERα Deficiency Did Not Affect Osteoclastogenesis

(A) TRAP-positive multinucleated cell count at 3 days after RANKL stimulation, cultured in 24-well plates (n = 6, N.S., not significant). Data are represented as mean ± SEM.

(B) TRAP staining and actin ring formation of RANKL induced primary cultured osteoclasts from bone-marrow cells of $ER\alpha^{+/+}$ and $ER\alpha^{\Delta Oc/\Delta Oc}$ mice.

(C) RT-PCR analysis of genes related to osteoclastogenesis.

(D) Western blot analysis of phosphorylated p38, JNK, and IκB of primary cultured bone-marrow cells stimulated with or without 100 ng/ml of RANKL for 15 min.

the search for candidate ERα target genes in bone by DNA microarray analysis (Figure S3), we found that a number of apoptosis-related factors were regulated by estrogen in the intact bone of $ER\alpha^{+/+}$ females but dysregulated in $ER\alpha^{\Delta Oc/\Delta Oc}$ females. This observation is consistent with a previous report of estrogen-induced apoptosis of mature osteoclasts (Kameda et al., 1997). Real-time RT-PCR to validate the estrogen regulations of the candidate genes revealed that gene expression of *FasL*, an apoptotic factor, was responsive to E2 (Figure 6A). Estrogen treatment (+E2) indeed induced expression of FasL protein in bone of ovariectomized $ER\alpha^{+/+}$, but this induction was not obvious in ovariectomized $ER\alpha^{\Delta Oc/\Delta Oc}$ mice (Figures 6B and 6C). Reflecting FasL induction by estrogen, estrogen-induced apoptosis (as observed by the TUNEL assay) in TRAP-positive mature trabecular osteoclasts in the distal femurs of the $ER\alpha^{+/+}$ mice was detected, but this E2 response was abolished in the $ER\alpha^{\Delta Oc/\Delta Oc}$ mice (Figure 6D). Furthermore, in mice lacking functional FasL ($FasL^{gld/gld}$), neither enhanced bone resorption nor bone mass loss was induced by ovariectomy (Figures 6E and 6F).

Osteoclastic ERα Mediates Estrogen-Induced apoptosis by FasL

The expression level of ERα protein in differentiated osteoclasts derived from bone marrow cells was very low, but induction of *FasL* gene expression was also detectable in the cultured osteoclasts of $ER\alpha^{+/+}$ females as well as males (Figure 7A). However, this E2 response was impaired in cultured osteoclasts from $ER\alpha^{\Delta Oc/\Delta Oc}$ females (Figure 7A). It is notable that such responses are also induced by tamoxifen (Figure 7C), which is an osteoprotective SERM (Harada and Rodan, 2003). ERα overexpression augmented *FasL* gene expression in response to estrogen in cultured osteoclasts from $ER\alpha^{\Delta Oc/\Delta Oc}$ females (Figure S4A). In primary cultured calvarial osteoblasts from females as well as males (Suzawa et al., 2003), *FasL* gene induction by E2 and tamoxifen was also seen; however, it was not accompanied by increased apoptosis (data not shown). Thus, it appears that estrogen-induced apoptosis in osteoclasts is mediated by FasL expression in osteoclasts in the trabecular bone areas, presumably as well as in osteoblasts in cortical bone areas. As expected, the cell number of TUNEL-positive osteoclasts was increased by E2 in the cultured osteoclasts from $ER\alpha^{+/+}$ females, but E2-induced apoptosis was undetectable in $ER\alpha^{\Delta Oc/\Delta Oc}$ osteoclasts (Figure 7B). Consistent with FasL-induced apoptosis, *Fas* gene expression was observed (Figure 7D), but it was likely that Fas expression did not require ERα function (Figures S4B and S4C). Expression levels of *Fas* and *ERα* as well as E2 response in apoptosis appeared to fluctuate during osteoclast differentiation (Figures S4B–S4D); however, in FasL mutant ($FasL^{gld/gld}$) females, the E2-induced apoptosis was abolished (Figure S4E). These findings suggest that activated ERα in differentiated osteoclasts induces apoptosis through activating FasL/Fas signaling. This leads to suppression of bone resorption through truncating the already short life span of differentiated osteoclasts (Teitelbaum, 2006).

DISCUSSION

Selective ablation of ERα in mature osteoclasts in female mice shows that the osteoprotective effect of estrogen is mediated by osteoclastic ERα, at least in the trabecular regions of the tibiae, femur, and lumbar vertebrae of female mice. Activated ERα by estrogen as well as SERMs appears to truncate the already short life span (estimated at 2 weeks) of differentiated osteoclasts by inducing apoptosis through activation of the Fas/FasL system.

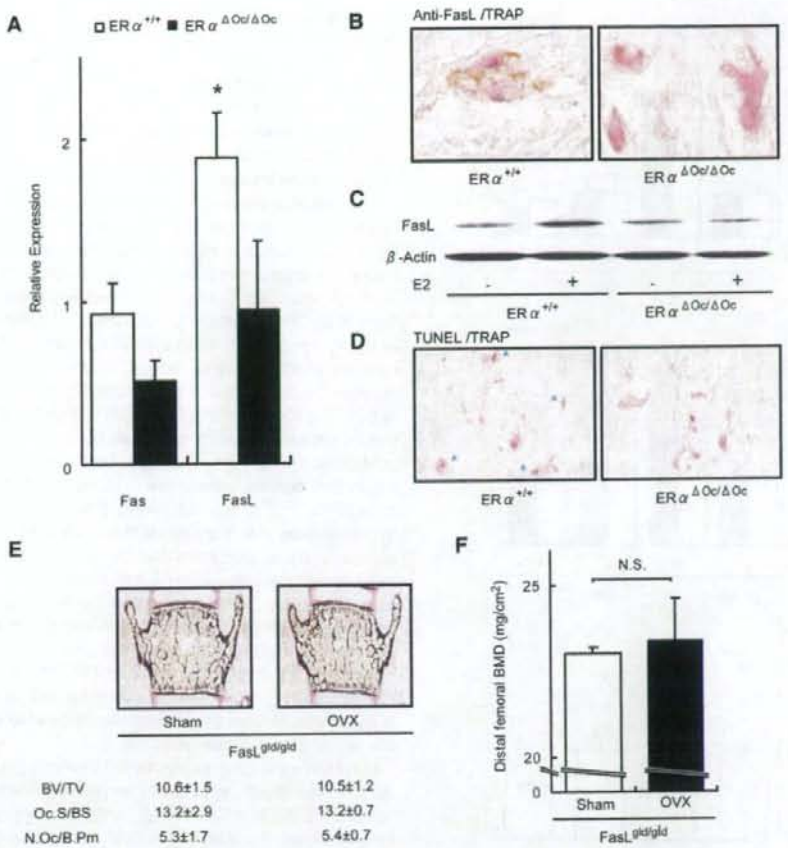

Figure 6. Activated ERα Induced Fas Ligand Expression and Apoptosis in Differentiated Osteoclasts of Intact Bone

(A) Real-time RT-PCR analysis of *Fas* and *FasL*. Expression levels in bones from E2-treated ovariectomized $ER\alpha^{+/+}$ (open column) and $ER\alpha^{\Delta Oc/\Delta Oc}$ (filled column) were compared with the ovariectomized groups of each genotype without E2 administration (*$p < 0.05$ compared to $ER\alpha^{+/+}$). Data are represented as mean ± SEM.

(B) Immunohistochemical analysis of anti-FasL with TRAP staining of the sections from the distal femurs of E2-treated ovariectomized $ER\alpha^{+/+}$ and $ER\alpha^{\Delta Oc/\Delta Oc}$ mice. Brawny stained cells are anti-FasL positive.

(C) Anti-FasL western blot analysis of proteins obtained from femurs of ovariectomized $ER\alpha^{+/+}$ and $ER\alpha^{\Delta Oc/\Delta Oc}$ mice treated with or without E2, using anti-β-actin as internal control.

(D) TUNEL staining with TRAP staining of the sections from the distal femurs of E2-treated ovariectomized $ER\alpha^{+/+}$ and $ER\alpha^{\Delta Oc/\Delta Oc}$ mice. Arrowheads indicate both TUNEL (brown)- and TRAP-positive staining cells.

(E) Bone histomorphometrical analysis of sham-operated or ovariectomized $FasL^{gld/gld}$ mice.

(F) BMD of the distal femurs of sham operated or ovariectomized $FasL^{gld/gld}$ mice. Data are represented as mean ± SEM.

This attenuates bone resorption. This idea is supported by previous observations that estrogen deficiency following menopause or ovariectomy leads to high bone turnover, particularly in the trabecular areas, as bone is rapidly lost through enhanced resorption (Delmas, 2002; Tolar et al., 2004). Thus, estrogen treatment leads to recovery from osteopenia by reducing resorption (Delmas, 2002; Rodan and Martin, 2000), partly by the induction of osteoclast cell death.

In contrast to the osteopenia seen in the $ER\alpha^{\Delta Oc/\Delta Oc}$ females, the $ER\alpha^{\Delta Oc/\Delta Oc}$ male mice unexpectedly had no bone loss. The male mice still demonstrated an ERα-mediated induction of FasL in response to estrogen with subsequent apoptosis of osteoclasts (Figure 7). Both male mice with a deficiency of aromatase that are unable to locally produce estrogen from testosterone and men with a genetic mutation in the *ERα* gene suffer from osteoporosis (Smith et al., 1994). Considering that the

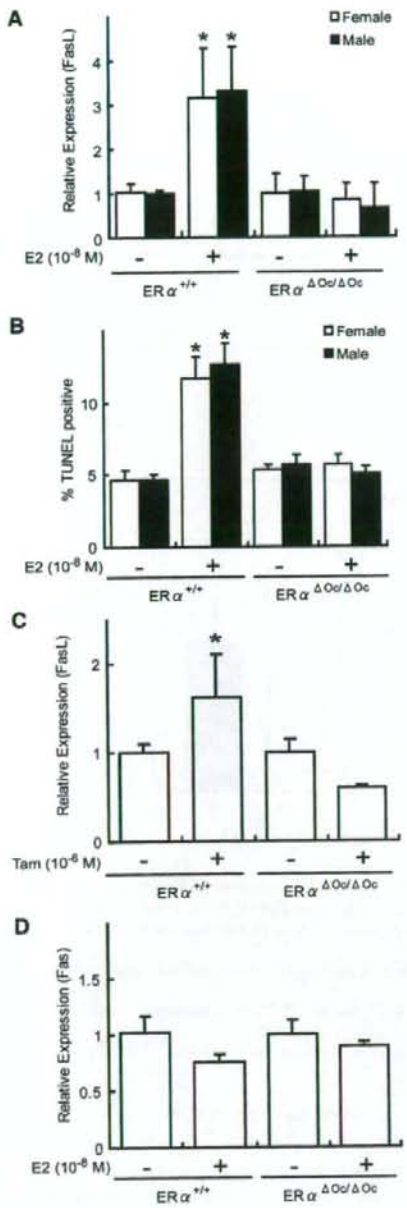

Figure 7. Estrogen-Induced *FasL* Expression and Apoptosis Required ERα in Cultured Osteoclasts

(A) Real-time RT-PCR analysis of *FasL* expression using total RNA obtained from in vitro primary cultured osteoclasts of each genotype at 3 days after RANKL stimulation, treated with or without E2 (10^{-8} M) for 4 hr (*$p < 0.05$ compared to the group treated without E2). Data are represented as mean ± SEM.

markedly elevated levels of testosterone in ERα KO females may be potent enough to maintain normal bone turnover (Syed and Khosla, 2005), it is likely that the activated AR might be functionally sufficient in male mice to compensate for the ERα deficiency in bone (Kawano et al., 2003). However, species differences in the osteoprotective action of sex steroid hormones still need to be carefully addressed.

Fas/FasL system-mediated apoptotic induction of osteoclasts by estrogen may well be a part of the mechanism for the antiresorptive action of estrogen and SERMs in trabecular bone areas (Delmas, 2002; Rodan and Martin, 2000; Simpson and Davis, 2001; Syed and Khosla, 2005; Tolar et al., 2004). Regulation of osteoclast differentiation is tightly coupled to osteoblastic function in terms of cytokine production and cell-cell contact (Karsenty and Wagner, 2002; Martin and Sims, 2005; Mundy and Elefteriou, 2006; Teitelbaum and Ross, 2003). Indeed, upregulation of osteoclastogenic cytokines by ovariectomy was unaffected in $ER\alpha^{\Delta Oc/\Delta Oc}$ females. Considering the observation that cortical bone mass is increased in ovariectomized $ER\alpha^{\Delta Oc/\Delta Oc}$ females during estrogen treatment, it is conceivable that the antiresorptive estrogen action in cortical bone is also mediated by osteoblastic ERα. In this regard, FasL induction by estrogen in osteoblasts may contribute to the osteoprotective estrogen action, and *FasL* gene induction by estrogen was in fact detected in primary cultured osteoblasts from female calvaria by us as well as another group (S. Krum and M. Brown, personal communication). Thus, similar experiments in which ERα is selectively ablated in osteoblasts are needed to define the role of ERα in these cells.

In osteoclastic cells, expression of the *FasL* gene, which leads to apoptosis, appears to be positive controlled by activated ERα. Not surprisingly, a direct binding site for ERα has been mapped in the *FasL* gene locus (S. Krum and M. Brown, personal communication). An osteoclast- and cell-differentiation stage-specific mechanism may underlie this gene induction in the *FasL* gene promoter. A recent study demonstrated that ERα recruitment to specific promoter sites of given ERα target genes was cell-type specific (Carroll et al., 2005). Thus, there is significant impetus to identify the osteoclastic factor that associates with ERα in the *FasL* gene promoter. Such identification will lead to a better understanding of the molecular basis of the osteoprotective estrogen action and provide a target against which to develop SERMs of greater effectiveness.

(B) Apoptotic cells were defined as those with TUNEL-positive nuclei among TRAP-positive multinucleated primary cultured osteoclasts treated with or without E2 (10^{-8} M) for 12 hr in 96-well plates (*$p < 0.05$ compared to the group treated without E2). Data are represented as mean ± SEM.

(C) *FasL* expression in each genotypic female osteoclastic cells treated with or without Tam (10^{-6} M) (*$p < 0.05$ compared to the group treated without Tam). Data are represented as mean ± SEM.

(D) Expression of *Fas* was measured as described in the legend of Figure 7A. Data are represented as mean ± SEM.

EXPERIMENTAL PROCEDURES

Ctsk-Cre Construction and Generation of the Knockin Mouse Lines

An RP23-422n18 BAC clone containing the mouse *Ctsk* gene was purchased from Invitrogen (Carlsbad, CA). The *FRT-Kan^r/Neo^r-FRT* and *nlsCre* fragments were obtained from plasmids pSK2/3-*FRT-Neo* and pIC-*Cre*. Two homologous arms of 500 bp from the *Ctsk* gene were inserted into both sides of the *nlsCre-FRT-Kan^r/Neo^r-FRT* cassette in the pSK2/3-*FRT-Neo* plasmid. The *nlsCre-FRT-Kan^r/Neo^r-FRT* cassette was introduced into the endogenous ATG start site of the *Ctsk* gene by recombineering approaches (Copeland et al., 2001). Targeted BAC was reduced in size from 189 kb to 26 kb and subcloned into the pMC1-DTpA vector by the gap-repair method. The targeted TT2 ES clones were selected after positive-negative selection with G418 and DT-A with Southern analysis, then aggregated with single eight-cell embryos from CD-1 mice (Yoshizawa et al., 1997). Chimeric mice were then crossed with a general deleter mouse line, *ACTB-Flpe* (Jackson Laboratory), to remove the *Kan^r/Neo^r* cassette. The *Ctsk-Cre* mice (*Ctsk$^{Cre/+}$*), originally on a hybrid C57BL/6 and CBA genetic background, were backcrossed for four generations into a C57BL/6J background. *FasL$^{gld/gld}$* mice were also purchased from Jackson Laboratory.

Analysis of Cre Recombinase Activities

Expression of the Cre transcript was detected by RT-PCR. Southern analysis using a *Cre* cDNA probe was performed with total RNA extracted from 12-week-old mice. To evaluate the specificity and efficiency of Cre-mediated recombination, we mated the *Ctsk$^{Cre/+}$* mice to *CAG-CAT-Z* reporter mice (kindly provided by J. Miyazaki) (Sakai and Miyazaki, 1997) and genotyped their offspring with *Cre*-specific primers. β-galactosidase activity of the expressed *LacZ* gene driven by the *CAG* promoter was expected to be detected in the given cells expressing functional Cre recombinase.

In Vitro Osteoclastogenesis and Ligand Application

Bone-marrow cells derived from 8-week-old mice were plated in culture dishes containing α-MEM (GIBCO-BRL) with 10% FBS (JRH) and 10 ng/ml M-CSF (Genzyme). After incubation for 48 hr, adherent cells were used as osteoclast precursor cells after washing out the nonadherent cells. Cells were cultured in the presence of 10 ng/ml M-CSF and 100 ng/ml RANKL (Peprotech) to generate osteoclast-like cells (Koga et al., 2004) for 3 days, so the total culture time was 5 days. Three days after RANKL stimulation, primary cultured osteoclasts were treated with 10^{-8} M of 17β-estradiol (E2) (Sigma-Aldrich Co.) or 10^{-6} M 4-hydroxytamoxifen (Tam) (Sigma-Aldrich Co.) in phenol-red free medium.

Generation of Osteoclast-Specific ERα KO Mice

The ERα conditional (*ERα$^{flox/flox}$*) (Dupont et al., 2000) and null alleles with a C57BL/6J background have been previously described. *ERα$^{flox/flox}$* mice were crossed with *Ctsk$^{Cre/+}$* mice to generate *Ctsk$^{Cre/+}$; ERα$^{flox/+}$* mice. *Ctsk$^{Cre/+}$; ERα$^{+/+}$* (*ERα$^{+/+}$*) and *Ctsk$^{Cre/+}$; ERα$^{flox/flox}$* (*ERα$^{\Delta Oc/\Delta Oc}$*) mice were obtained by crossing *Ctsk$^{Cre/+}$; ERα$^{flox/-}$* with *ERα$^{flox/+}$* mouse lines.

Radiological Analysis

Bone radiographs of the femurs of 12-week-old *Ctsk$^{Cre/+}$; ERα$^{flox/flox}$* (*ERα$^{\Delta Oc/\Delta Oc}$*) and *Ctsk$^{Cre/+}$; ERα$^{+/+}$* (*ERα$^{+/+}$*) littermates were visualized with a soft X-ray apparatus (TRS-1005: SOFTRON). BMD was measured by DXA using a bone mineral analyzer (DCS-600EX: ALOKA). Micro Computed Tomography scanning of the femurs was performed using a composite X-ray analyzer (NX-CP-C80H-IL: Nittetsu ELEX Co.) (Kawano et al., 2003). Tomograms were obtained with a slice thickness of 10 μm and reconstructed at 12 × 12 pixels into a 3D image by the volume-rending method (VIP-Station; Teijin System Technology) using a computer.

Analysis of Skeletal Morphology

Twelve-week-old *Ctsk$^{Cre/+}$; ERα$^{flox/flox}$* (*ERα$^{\Delta Oc/\Delta Oc}$*) and *Ctsk$^{Cre/+}$; ERα$^{+/+}$* (*ERα$^{+/+}$*) littermates were double labeled with subcutaneous injections of 16 mg/kg of calcein (Sigma) at 4 and 2 days before sacrifice. Tibiae were removed from each mouse and fixed with 70% ethanol. They were stained with Villanueva bone stain for 7 days and embedded in methyl-methacrylate (Wako) (Yoshizawa et al., 1997). Frontal plane sections (5-μm thick) of the proximal tibia were cut using a Microtome (LEICA). The cancellous bone was measured in the secondary spongiosa located 500 μm from the epiphyseal growth plate and 160 μm from the endocortical surface (Kawano et al., 2003; Nakamichi et al., 2003). Bone histomorphometric measurements of the tibia were made using a semiautomatic image analyzing system (System Supply) and a fluorescent microscope (Optiphot; Nikon). Similar measurements of the lumbar vertebral bodies were done as previously reported (Takeda et al., 2002). Standard bone histomorphometrical nomenclatures, symbols, and units were used as described in the report of the ASBMR Histomophometry Nomenclature Committee.

Ovariectomy and Hormone Replacement

Female *Ctsk$^{Cre/+}$; ERα$^{flox/flox}$* (*ERα$^{\Delta Oc/\Delta Oc}$*) and *Ctsk$^{Cre/+}$; ERα$^{+/+}$* (*ERα$^{+/+}$*) littermates were ovariectomized or sham operated at 8–12 weeks of age for 2 weeks for all experiments, and slow releasing pellets of E2 (0.83 μg/day) or placebo (Innovative Research, Sarasota, FL) were implanted subcutaneously in the scapular region behind the neck (Sato et al., 2004; Shiina et al., 2006).

Immunohistochemistry

Twelve-week-old *Ctsk$^{Cre/+}$; ERα$^{flox/flox}$* (*ERα$^{\Delta Oc/\Delta Oc}$*) and *Ctsk$^{Cre/+}$; ERα$^{+/+}$* (*ERα$^{+/+}$*) littermates were fixed with 4% PFA by perfusion. Serial sections of the brain (20 μm thick) were divided into two groups and used for single labeling for the ERα or thionin to allow determination of the areas to be measured. Tibiae and femurs were decalcified in 10% EDTA for 2–4 weeks after fixation and then embedded in paraffin sections. Sections were incubated in L.A.B. solution (Polysciences) for 30 min to retrieve antigen. The cooled sections were incubated in 1% H_2O_2 for 30 min to quench endogenous peroxidase and then washed with 1% Triton X-100 in PBS for 10 min. To block nonspecific antibody binding, sections were incubated in blocking solution (DAKO) for 5 min. Sections were then incubated with anti-ERα (Santa Cruz, CA) and anti-FasL (Santa Cruz, CA) in blocking solution overnight at 4°C. Staining was then performed using the EnVision+ HRP System (Dako) and 3, 3′-diaminobendizine tetrahydrochloride substrate (Sigma), counterstained with TRAP, dehydrated through an ethanol series and xylene, before mounting (Sato et al., 2004).

ERα Overexpression

Two days after RANKL stimulation, an expression vector of mouse ERα was tranfected into immature osteoclastic cells from *ERα$^{\Delta Oc/\Delta Oc}$* mice using Superfect (QIAGEN) as manufacture's instruction.

Real-Time RT-PCR

One microgram of total RNA from each sample was reverse transcribed into first-strand cDNA with random hexamers using Superscript III reverse transcriptase (Invitrogen). Primer sets for all genes were purchased from Takara Bio. Inc. (Tokyo, Japan). Real-time RT-PCR was performed using SYBR Premix Ex Taq (Takara) with the ABI PRISM 7900HT (Applied Biosystems) according to the manufacturer's instructions. Experimental samples were matched to a standard curve generated by amplifying serially diluted products using the same PCR protocol. To correct for variability in RNA recovery and efficiency of reverse transcription, *Gapdh* cDNA was amplified and quantified in each cDNA preparation. Normalization and calculation steps were performed as reported previously (Takezawa et al., 2007).